Computer-Aided Design 45 (2013) 639–656

Contents lists available at SciVerse ScienceDirect

Computer-Aided Design

journal homepage: www.elsevier.com/locate/cad

Improving Nagata patch interpolation applied for tool surface description in sheet metal forming simulation

D.M. Neto [a,*], M.C. Oliveira [a], L.F. Menezes [a], J.L. Alves [b]

[a] CEMUC, Department of Mechanical Engineering, University of Coimbra, Polo II, Rua Luís Reis Santos, Pinhal de Marrocos, 3030-788 Coimbra, Portugal

[b] CT2M, Department of Mechanical Engineering, University of Minho, Campus de Azurém, 4800-058 Guimarães, Portugal

ARTICLE INFO

Article history:
Received 15 July 2011
Accepted 22 October 2012

Keywords:
Nagata patch
Local interpolation
Tool modelling
Normal vector approximation
Sheet metal forming

ABSTRACT

The contact surface description is a very important field in the numerical simulation of problems involving frictional contact, which are among the most difficult ones in continuum mechanics, as is the case of sheet metal forming simulation. In this paper, a methodology to control the Nagata patch interpolation of piecewise linear meshes is proposed, in order to improve its applicability for tool surface description used in the numerical simulation of sheet metal forming processes. The interpolation can be applied either to triangular and quadrilateral Nagata patches, as well as structured and unstructured patches. The normal vectors needed for the Nagata interpolation are obtained through two distinct strategies. The first uses the information available in the CAD surface model, while the second resorts only to the piecewise linear mesh model information. In order to evaluate the interpolation accuracy, the Nagata patch is applied to describe a sheet metal forming complex shape part tool geometry. The results obtained show that, regardless of the strategy used to evaluate the surface normal vectors, the use of the proposed Nagata patch interpolation enables a large improvement in the geometric accuracy when compared with the models composed by piecewise linear elements. The use of CAD surface geometry to evaluate the surface normal vectors leads to the best Nagata patch interpolation in terms of shape and normal vector field accuracy.

1. Introduction

The sheet metal forming process is widely used in several industrial areas, particularly in the automotive industry, to produce large quantities of sheet metal components such as inner parts, stiffeners and outer body panels. The quality of the product part is dictated by the tools design, process parameters, shape and material of the blank. Since the manufacturing of forming tools is both costly and time consuming, they play a central role in the global cost of a stamped part. The industrial desires for reducing both the conception time and the cost associated to the trial-and-error forming tools design process, has led to the mandatory application of the finite element method to perform the virtual try-out. [1,2]. In fact, this virtual try-out process permits an enormous time and cost reduction in the die design process [3], since it allows to predict the deformed shape of blank, the thickness and strain distribution, and even defects such as fracture, necking and wrinkles [4]. During the last years, the growing increase of computer technology has led to the decrease of computer time and memory requirements. At the same time, significant attention has been devoted to increase the accuracy and robustness of the algorithms in order to achieve reliable sheet metal forming numerical simulation results [5–7]. In order to take advantage of the recent multi-core processors, several high performance computing techniques have been incorporated in the computational applications in order to increase their speed-up [8,9]. These improvements allow combining the numerical simulation with optimization procedures, which typically require a great number of iterations to achieve a solution and, subsequently, high computation times [10].

The finite element model used in the numerical simulation of sheet metal forming processes is usually divided in two parts: the metal sheet and the forming tools [11]. In a wide range of technological processes, it is possible to assume that the forming tools behave as rigid bodies. Therefore, the model can consider only the outer surfaces of the tool as contact surfaces. On the other hand, the deformable body (metal sheet) is usually discretized with the aid of a finite element mesh, on which all numerical variables involved in the simulation are evaluated. Recently, Hughes et al. [12] proposed the concept of isogeometric analysis, which employ NURBS to represent the geometry of the deformable body and uses the NURBS shape function to approximate the field variables, avoiding the use

* Correspondence to: Department of Mechanical Engineering, University of Coimbra, Polo II, Rua Luís Reis Santos, Pinhal de Marrocos, 3030-788 Coimbra, Portugal. Tel.: +351 239790700; fax: +351 239790701.

E-mail addresses: diogo.neto@dem.uc.pt (D.M. Neto), marta.oliveira@dem.uc.pt (M.C. Oliveira), luis.menezes@dem.uc.pt (L.F. Menezes), jlalves@dem.uminho.pt (J.L. Alves).

0010-4485/$ – see front matter © 2012 Elsevier Ltd. All rights reserved.
doi:10.1016/j.cad.2012.10.046

of the classic finite element mesh. The application of this new concept in problems involving large deformation and frictional contact can lead to improved results in contact treatment, since it uses the exact geometry. However, some difficulties arise due to the nonlinear nature of contact problems [13]. In fact, the numerical simulation of sheet metal forming processes always comprises the following three nonlinearities: geometric, material and frictional contact, which are solved using incremental-iterative solution procedures. However, the numerical treatment of the interactions resulting from the frictional contact between the sheet and the forming tools is quite challenging in terms of robustness issues, due to the extremely nonlinear and non-smooth character of the contact operators [14,15]. During the forming process, the boundary conditions resulting from contact are constantly changing. Therefore, the contact status of every deformable body node candidate to establish contact with the forming tools, needs to be updated in each increment. This procedure starts with the so-called contact search algorithm, which should identify for each node candidate to establish contact, the position point on the tool surface where contact can occur. Typically the contact search algorithm is divided into two phases: global and local search [16,17]. In each increment, the contact status of every node also needs to be updated during the iterative procedure, by applying the local search algorithm. Therefore, the computational effort associated to the contact search algorithm strongly influences the computation time. In fact, recent studies showed that the computational time demanded by the local search is about 90% of the total time spend in the contact search [18]. The main task involved in this phase is the projection of each candidate node onto the tool surface, which implies solving a nonlinear system of equations.

The accurate description of the tool geometry is a very important issue to take into account in the numerical simulation of forming processes, particularly in the analysis of springback phenomena [19] and also in processes where the contact area is quite small with respect to the component size [20]. In case of rigid tools, several schemes have been developed to define the tool surfaces geometry, which can be categorized in four schemes: (i) the analytical function; (ii) the finite element mesh, (iii) the piecewise linear mesh, and (iv) the parametric patch [21]. The first scheme is very useful for simple tool geometries, since it is composed by an assembly of simple analytical shapes [21,22]. However, this scheme is unfeasible for more complex models, leading to the need to apply either the finite element mesh scheme or the piecewise linear approximation, both requiring a disproportionately finer mesh in curved areas in order to obtain a proper tool description [23]. Nevertheless, the artificial non-smoothness of the contact surfaces described by both schemes leads to artificial oscillations in the contact forces, non-realistic pressure jumps, contact cycling and can also lead to the divergence of the iterative procedure [24,25]. Hence, to overcome these types of problems, different strategies have been proposed to smoothly interpolate the given piecewise linear mesh, leading to significant improvements in the solution accuracy [26,27]. Typically, this operation involves the application of parametric patches in the surface description, such as Bézier [28], B-spline [29,30] and NURBS [25]. Nevertheless, since these interpolation methods were originally developed for 2D problems, their extension for 3D surfaces has the inherent disadvantage that they cannot represent surfaces with arbitrary mesh typology/topology. In this context, Puso and Laursen [31] proposed a method using Gregory patches to smooth the contact surfaces in 3D problems, which is suitable for unstructured meshes of quadrilaterals. However, all the smoothing methods presented above have in common the high order of the interpolation adopted, which leads to higher computational cost, due to the higher complexity of the local search procedure [32]. The other possible strategy to use the parametric patch scheme is applying directly the model delivered from the CAD system. Trimmed NURBS patches are commonly used in CAD systems due to the natural difficultly of defining complex geometries with untrimmed patches [33]. Hence, the algorithms required to deal with trimmed patches are computationally more expensive, since each patch presents a different validity domain, which must be stored in memory. Furthermore, CAD models are known to be plagued by geometrical or topological errors and inconsistencies. Therefore, before using the model it is always necessary to perform some geometry repair, clean-up, and preparation. This laborious, manual-intervention process is the rule, rather than the exception. Must CAD model errors and inconsistencies (e.g., gaps/overlaps between abutting surfaces) result from the lack of a robust solution to the surface intersection problem. In fact, there is no satisfactory theory on how to approximate the intersection curve and, consequently, the trimmed surfaces [34]. Therefore, currently the direct application of CAD models in finite element numerical simulation requires a previous treatment of model, which limits its application only to academic environment [35]. In fact, it is not easy to avoid the CAD model errors and inconsistencies and, consequently, circumvent the geometry repair step. Although, meshing algorithms have attained a high degree of sophistication and reliability, they basically reproduce the information available in the CAD model [34]. The adoption of the piecewise linear scheme combined with a smoothing technique reduces the amount of operations involved in the geometry repair step.

Recently, Nagata [36] proposed a new algorithm to interpolate surfaces, which can be considered a smoothing technique for piecewise linear meshes using parametric patches. The central idea of the Nagata patch is the quadratic interpolation of a curved segment, from the position and normal vectors at the end points. The principal advantage of this method over the existing ones is its ability to recover the surface curvature of models discretized by both triangular and quadrilateral facets, as well as allowing the use of structured and unstructured meshes. Besides, the biquadratic patch degree (minimum required to describe a curve) allows reducing the computational cost associated to the local search algorithm, while the geometric accuracy attained is acceptable even with a small amount of patches. The application of this smoothing technique in tool surface description assures C^1 continuity in the vertices and *quasi*-C^1 in the edges between patches [20,36]. Therefore, this method can be considered as slightly more complex than the piecewise linear approximation and almost as accurate as the CAD representation. The main drawback of this method is its incapacity to describe patches which present inflection points, since the interpolation degree is only two. Thus, for particular cases, the algorithm can result in the inversion of the patch orientation in conjunction with a very sharp bending. This situation is prohibited when applied to tool surface description, since it will lead to convergence problems in the local contact search algorithm. Thus, the main subject of this work is defining strategies to overcome this type of problems. Moreover, some schemes to evaluate the required vertex normal vector are presented and compared.

In this study, the original Nagata patch interpolation algorithm is analyzed in order to better control its application for smoothing piecewise linear meshes, used to describe the rigid contact surfaces in sheet metal forming simulation. Thus, in the next section the Nagata patch formulation for both triangular and quadrilateral patches is briefly presented, in order to introduce the method proposed to control the instabilities in the Nagata patches interpolation. Afterwards, the Nagata patch interpolation is applied to represent a circular arc and the interpolation accuracy is evaluated using the radial and normal vector errors. Section 4 presents two approaches that can be applied to evaluate the normal vector in each vertex of the piecewise mesh. One of the

approaches uses the information of the surface geometry available in CAD model, while the other uses only the information available in the piecewise mesh. For this last approach, a methodology to improve the normal vector approximation is proposed. Section 5 details the application of the Nagata patch interpolation to describe a complex sheet metal forming tool. Both approaches, to evaluate the normal vector in each vertex, are employed in the Nagata patch interpolation and compared. The accuracy of the Nagata patch interpolation is evaluated through the shape and normal vector errors and compared with the one achieved by the model composed by piecewise linear elements, in order to highlight its unique features for sheet metal forming tools description. Finally, the main conclusions are summarized in Section 6.

2. Nagata patch formulation

Nagata [36] proposed a simple method for interpolating surfaces discretized with piecewise linear elements in order to recover the original geometry with good accuracy. Its simplicity comes from the reduced interpolation degree and it requires only the position and normal vectors in each vertex of the discretized surface model. The interpolation of an edge is replaced by a curve in the form:

$$\mathbf{x}(\xi) = \mathbf{x}_0 + (\mathbf{x}_1 - \mathbf{x}_0 - \mathbf{c})\xi + \mathbf{c}\xi^2, \tag{1}$$

where ξ is the local coordinate that satisfies the condition $0 \leq \xi \leq 1$, and $\mathbf{x}_0$ and $\mathbf{x}_1$ are the position vectors of the edge ends. The derivative of the Nagata curve, given in Eq. (1), is:

$$\mathbf{x}_\xi(\xi) \equiv \frac{\mathrm{d}\mathbf{x}}{\mathrm{d}\xi} = (\mathbf{x}_1 - \mathbf{x}_0) + (2\xi - 1)\mathbf{c}, \tag{2}$$

which should be orthogonal to the unit normal vectors $\mathbf{n}_0$ and $\mathbf{n}_1$ at the end points, i.e. satisfies the boundary conditions. The derivative of the curve gives the tangential direction, necessary to calculate the normal direction at each point on the Nagata curve.

The coefficient $\mathbf{c}$, presented in Eqs. (1) and (2), adds the curvature to the edge. Assuming that the curve given by Eq. (1) is orthogonal to the normal vectors $\mathbf{n}_0$ and $\mathbf{n}_1$ at $\mathbf{x}_0$ and $\mathbf{x}_1$, respectively, the vector $\mathbf{c}$ can be determined, minimizing its norm, as follows:

$$\mathbf{c}(\mathbf{x}_0, \mathbf{x}_1, \mathbf{n}_0, \mathbf{n}_1) = \begin{cases} \dfrac{[\mathbf{n}_0, \mathbf{n}_1]}{1-a^2} \begin{bmatrix} 1 & -a \\ -a & 1 \end{bmatrix} \begin{Bmatrix} \mathbf{n}_0 \cdot (\mathbf{x}_1 - \mathbf{x}_0) \\ -\mathbf{n}_1 \cdot (\mathbf{x}_1 - \mathbf{x}_0) \end{Bmatrix} & (a \neq \pm 1) \\ \dfrac{[\mathbf{n}_0, \pm\mathbf{n}_0]}{2} \begin{Bmatrix} \mathbf{n}_0 \cdot (\mathbf{x}_1 - \mathbf{x}_0) \\ \mp\mathbf{n}_0 \cdot (\mathbf{x}_1 - \mathbf{x}_0) \end{Bmatrix} = \mathbf{0} & (a = \pm 1), \end{cases} \tag{3}$$

where $a = \mathbf{n}_0 \cdot \mathbf{n}_1$, is the cosine of the angle between the two end edge normal vectors and $[\mathbf{n}_0, \mathbf{n}_1]$ represents a matrix with the first column equal to vector $\mathbf{n}_0$ and the second equal to vector $\mathbf{n}_1$. At the first step of the Nagata interpolation, each edge of the piecewise facet is independently interpolated, and then the interior of the patch is filled reproducing the boundary conditions. Since the triangular and quadrilateral typologies of the piecewise facets are the most usual in surface description methods, in the following subsections the interpolation process is described for these Nagata patches.

2.1. Triangular patches

Consider the triangular patch presented in Fig. 1(a). The curvature of a piecewise linear element can be recovered by interpolating each edge with the polynomial given by Eq. (1). The input data necessary in the vertices v_1, v_2 and v_3 are the vectors corresponding to the position $\mathbf{x}_{00}$, $\mathbf{x}_{10}$ and $\mathbf{x}_{11}$, and to the normal $\mathbf{n}_{00}$, $\mathbf{n}_{10}$, $\mathbf{n}_{11}$, respectively. In case of a triangular patch, the

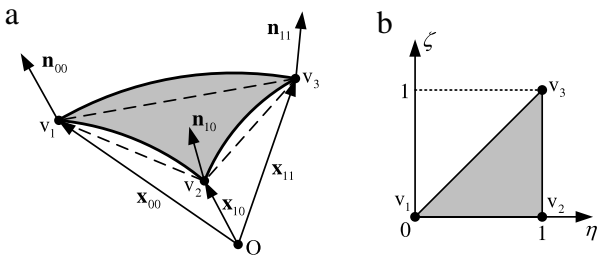

Fig. 1. Triangular Nagata patch interpolation: (a) sketch; (b) patch domain defined in its local coordinates.

interpolated surface is approximated by the following quadratic polynomial:

$$\mathbf{x}(\eta, \zeta) = \mathbf{c}_{00} + \mathbf{c}_{10}\eta + \mathbf{c}_{01}\zeta + \mathbf{c}_{11}\eta\zeta + \mathbf{c}_{20}\eta^2 + \mathbf{c}_{02}\zeta^2, \tag{4}$$

where $\mathbf{x}(\eta, \zeta)$ denotes the position vector of any point on the patch. The triangular patch domain is defined in the local coordinates η and ζ satisfying the condition $0 \leq \zeta \leq \eta \leq 1$, as shown in Fig. 1(b). The coefficient vectors of Eq. (4) are given by:

$$\begin{aligned} \mathbf{c}_{00} &= \mathbf{x}_{00}, \\ \mathbf{c}_{10} &= \mathbf{x}_{10} - \mathbf{x}_{00} - \mathbf{c}_1, \\ \mathbf{c}_{01} &= \mathbf{x}_{11} - \mathbf{x}_{10} + \mathbf{c}_1 - \mathbf{c}_3, \\ \mathbf{c}_{11} &= \mathbf{c}_3 - \mathbf{c}_1 - \mathbf{c}_2, \\ \mathbf{c}_{20} &= \mathbf{c}_1, \\ \mathbf{c}_{02} &= \mathbf{c}_2, \end{aligned} \tag{5}$$

where $\mathbf{c}_1$, $\mathbf{c}_2$ and $\mathbf{c}_3$ are the vectors defined by Eq. (3) for the edges $(\mathbf{x}_{00}, \mathbf{x}_{10})$, $(\mathbf{x}_{10}, \mathbf{x}_{11})$ and $(\mathbf{x}_{00}, \mathbf{x}_{11})$, respectively.

Partial differentiation of Eq. (4) is given by the following expressions:

$$\mathbf{x}_\eta(\eta, \zeta) \equiv \frac{\partial \mathbf{x}}{\partial \eta} = \mathbf{c}_{10} + \mathbf{c}_{11}\zeta + 2\mathbf{c}_{20}\eta, \tag{6}$$

$$\mathbf{x}_\zeta(\eta, \zeta) \equiv \frac{\partial \mathbf{x}}{\partial \zeta} = \mathbf{c}_{01} + \mathbf{c}_{11}\eta + 2\mathbf{c}_{02}\zeta, \tag{7}$$

which are required for evaluating the normal vector at any arbitrary location on the patch.

2.2. Quadrilateral patches

The quadrilateral patch represented in Fig. 2(a) is interpolated in a similar way as for the triangular patch. The necessary input data for the vertices v_1, v_2, v_3 and v_4 are the position vectors $\mathbf{x}_{00}$, $\mathbf{x}_{10}$, $\mathbf{x}_{11}$ and $\mathbf{x}_{01}$, and the unit normal vectors $\mathbf{n}_{00}$, $\mathbf{n}_{10}$, $\mathbf{n}_{11}$ and $\mathbf{n}_{01}$, respectively. The vertices do not need to be coplanar. The surface equation for quadrilateral patches is given by:

$$\begin{aligned} \mathbf{x}(\eta, \zeta) = {} & \mathbf{c}_{00} + \mathbf{c}_{10}\eta + \mathbf{c}_{01}\zeta + \mathbf{c}_{11}\eta\zeta + \mathbf{c}_{20}\eta^2 + \mathbf{c}_{02}\zeta^2 \\ & + \mathbf{c}_{21}\eta^2\zeta + \mathbf{c}_{12}\eta\zeta^2, \end{aligned} \tag{8}$$

where the patch domain in the local coordinates η and ζ is defined as $0 \leq \eta, \zeta \leq 1$ (see Fig. 2(b)). The coefficient vectors in Eq. (8) are given by:

$$\begin{aligned} \mathbf{c}_{00} &= \mathbf{x}_{00}, \\ \mathbf{c}_{10} &= \mathbf{x}_{10} - \mathbf{x}_{00} - \mathbf{c}_1, \\ \mathbf{c}_{01} &= \mathbf{x}_{01} - \mathbf{x}_{00} - \mathbf{c}_4, \\ \mathbf{c}_{11} &= \mathbf{x}_{11} - \mathbf{x}_{10} - \mathbf{x}_{01} + \mathbf{x}_{00} + \mathbf{c}_1 - \mathbf{c}_2 - \mathbf{c}_3 + \mathbf{c}_4, \\ \mathbf{c}_{20} &= \mathbf{c}_1, \\ \mathbf{c}_{02} &= \mathbf{c}_4, \\ \mathbf{c}_{21} &= \mathbf{c}_3 - \mathbf{c}_1, \\ \mathbf{c}_{12} &= \mathbf{c}_2 - \mathbf{c}_4, \end{aligned} \tag{9}$$

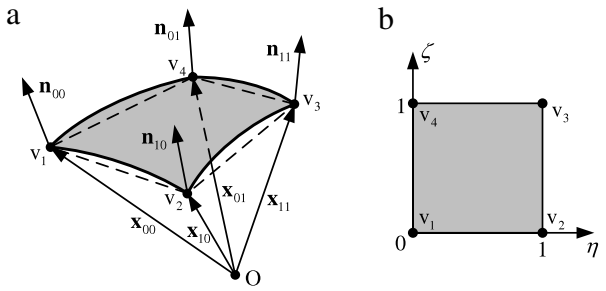

Fig. 2. Quadrilateral Nagata patch interpolation: (a) sketch; (b) patch domain defined in its local coordinates.

where $\mathbf{c}_1$, $\mathbf{c}_2$, $\mathbf{c}_3$ and $\mathbf{c}_4$ are the vectors defined by Eq. (3) for the edges $(\mathbf{x}_{00}, \mathbf{x}_{10})$, $(\mathbf{x}_{10}, \mathbf{x}_{11})$, $(\mathbf{x}_{01}, \mathbf{x}_{11})$ and $(\mathbf{x}_{00}, \mathbf{x}_{01})$, respectively.

Partial differentiation of Eq. (8) is given by the following expressions:

$$\mathbf{x}_\eta(\eta, \zeta) \equiv \frac{\partial \mathbf{x}}{\partial \eta} = \mathbf{c}_{10} + \mathbf{c}_{11}\zeta + 2\mathbf{c}_{20}\eta + 2\mathbf{c}_{21}\eta\zeta + \mathbf{c}_{12}\zeta^2, \tag{10}$$

$$\mathbf{x}_\zeta(\eta, \zeta) \equiv \frac{\partial \mathbf{x}}{\partial \zeta} = \mathbf{c}_{01} + \mathbf{c}_{11}\eta + 2\mathbf{c}_{02}\zeta + \mathbf{c}_{21}\eta^2 + 2\mathbf{c}_{12}\eta\zeta. \tag{11}$$

It should be mentioned that the above formulation can also be extended to other general n-sided patches. However, the triangular and quadrilateral piecewise facets are the most commonly used by the mesh generator codes to describe surfaces of arbitrary geometry [37].

2.3. Controlling the Nagata patch interpolation

In order to apply the Nagata patches interpolation to describe the tool surfaces employed in the numerical simulation of sheet metal forming process, the interpolation algorithm must be robust to ensure the efficiency of the contact search algorithm, the numerical stability and good convergence speed of the numerical simulations. The Nagata patch interpolation is a very flexible shape modeling algorithm that can lead to very sharp surfaces, which are undesirable and prejudicial when applied to frictional contact problems. Therefore, some restrictions should be added to the original formulation with the aim of avoiding the occurrence of these cases, always retaining the central idea of the simple quadratic interpolation originally proposed [36,38].

A single Nagata patch has no ability to describe a curve or surface with inflection points due to its quadratic formulation. Therefore, ideally during the discretization process, vertices should be associated to all inflection points, in order to accurately define the Nagata patch boundaries [39]. Fig. 3 shows an example of a curve with an inflection point interpolated employing the Nagata patch algorithm. It is visible that the attained approximation presents an inversion of the curve orientation near to the vertex. This type of solution is prohibited when using the Nagata patch interpolation method to describe tool surfaces, since it does not accurately represents the surface and, moreover, it will lead to severe convergence problems in the local contact search procedure.

The application of the Nagata patch interpolation, both for curve and surface descriptions, requires the information concerning the position vector and the surface normal vector in each vertex, as well as the connectivity of each piecewise element. The position vectors and the connectivity can be obtained from the piecewise linear approximation of the surface geometry under study, which can be composed by either triangular or quadrilateral elements. The surface normal vector definition requires information that is unavailable in the piecewise linear

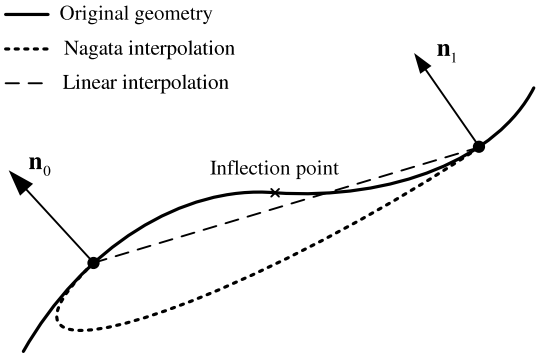

Fig. 3. Nagata interpolation applied to a curve presenting an inflection point between the two end points.

mesh. When this information is not available, it is necessary to determine a surface normal approximation, which results in a Nagata patch interpolation dictated by the new inputs (vertex normal vectors). The approximation of the normal vectors can lead to Nagata interpolations with high curvature gradient near to the vertices, which is undesirable for contact search algorithms.

As previously mentioned, the existence of Nagata patch interpolations with inversion of curve orientation or high localized curvature, are prohibited in the problem under analysis. An alternative to overcome these problems, without compromising too much the accuracy and keeping the information about the vertices position and their normal vectors, is to adopt the linear interpolation, as shown in Fig. 3 through the straight dashed line. This solution was already proposed by Boschiroli et al. [40] to solve the instability problems of the Nagata interpolation algorithm, in order to apply this type of patches in computer graphics. In their work, the authors highlight the localized problems associated to the original Nagata interpolation, when applied to complex piecewise meshes.

The original formulation, presented in the previous section, is characterized by an algebraic singular case ($a = \pm 1$, in Eq. (3)), which results in a linear interpolation, since $\mathbf{c}$ is equal to the null vector. This singular interpolation case does not satisfy the imposed boundary conditions, i.e., the Nagata patch is not orthogonal to the normal vectors given at the end points. Hence, the proposed improvements to the original Nagata patch interpolation algorithm consist on extending the singular case domain. This extension is performed in order to prevent interpolations with a high curvature variation, but keeping the original quadratic interpolation in the maximum number of patches as possible.

The strategy adopted in [40] to extend the singular case domain is based only in the value of parameter a (see Eq. (3)), which only depends on the angle between the normal vectors at the end points of each edge. In this study, the Nagata patch instability is identified through the normal vectors at the end points and also using the following normalized vector:

$$\mathbf{b} = \frac{\mathbf{x}_1 - \mathbf{x}_0}{|\mathbf{x}_1 - \mathbf{x}_0|}, \tag{12}$$

which has the direction of the vector joining the end points. The presence of inflection points in the original geometry is identified using the values of the angles between the normal end point vectors and the vector $\mathbf{b}$. When both vertex normal vectors contain the same orientation relatively to vector $\mathbf{b}$, i.e. the angle between each normal vector and $\mathbf{b}$ is smaller (Fig. 4(a)) or higher than 90° (Fig. 4(b)), then the original geometry presents a inflection point between the end points. This situation verifies the following condition:

$$(\mathbf{n}_0 \cdot \mathbf{b})(\mathbf{n}_1 \cdot \mathbf{b}) \geq 0, \tag{13}$$

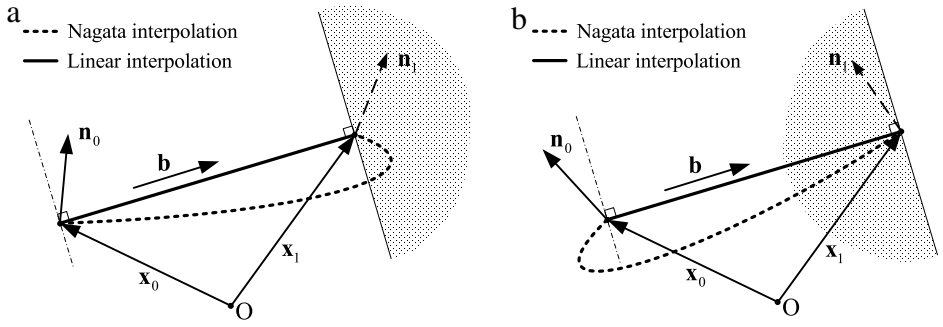

Fig. 4. Controlling the Nagata patch interpolation when both normal vectors present, relatively to the vector **b**: (a) the same orientation ($\mathbf{n}_0 \cdot \mathbf{b} \geq 0$ and $\mathbf{n}_1 \cdot \mathbf{b} \geq 0$); (b) opposite orientation ($\mathbf{n}_0 \cdot \mathbf{b} \leq 0$ and $\mathbf{n}_1 \cdot \mathbf{b} \leq 0$). Linear interpolation is applied if the normal vector $\mathbf{n}_1$ is located in the shaded zone.

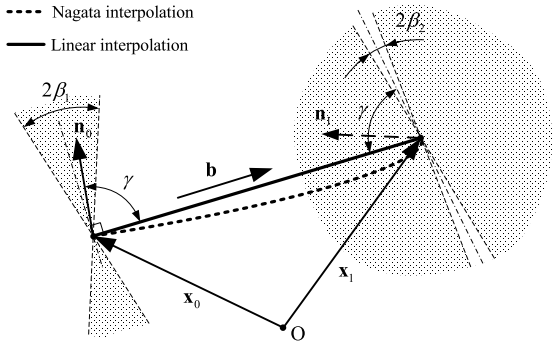

Fig. 5. Controlling the Nagata patch interpolation when the normal vector of one vertex is nearly perpendicular to vector **b** and the other one is away from the orthogonal position. Linear interpolation is applied if the normal vectors are located in a corresponding shaded zone.

which represents the multiplication of the dot products between the normal vectors and the vector joining the end points. The shaded zone in Fig. 4 represents the region where the normal vector $\mathbf{n}_1$ should be located, according to Eq. (13), in order to adopt the singular case, i.e. linear interpolation.

The second instability problem of the Nagata patch interpolation, mainly occurs when the normal vectors in the vertices are determined using an approximation method, and can be also identified by the relative orientation between the normal vectors and the vector **b**. When the evaluated normal vector of one vertex is nearly perpendicular to the vector **b** and the other one is away from the orthogonal position, as shown in Fig. 5, then it is highly probable that the Nagata interpolation will present a strong localized change in curvature. The interpolation of this edge is included into the singular case domain, when the following conditions are verified:

$$(|\mathbf{n}_0 \cdot \mathbf{b}| < \varepsilon_1 \vee |\mathbf{n}_1 \cdot \mathbf{b}| < \varepsilon_1) \wedge |(\mathbf{n}_0 \cdot \mathbf{b}) + (\mathbf{n}_1 \cdot \mathbf{b})| > \varepsilon_2. \quad (14)$$

ε_1 and ε_2 are coefficients proportional to the angles β_1 and β_2 (see Fig. 5), respectively. Since these coefficients present small values, the following relationships are valid:

$$\begin{aligned} \beta_1 &= \sin^{-1}(\varepsilon_1) \cong \varepsilon_1, \\ \beta_2 &= \frac{1}{2}\left(\sin^{-1}(\varepsilon_1 + \varepsilon_2) - \sin^{-1}(\varepsilon_1 - \varepsilon_2)\right) \cong \varepsilon_2. \end{aligned} \quad (15)$$

The angle β_1 limits the position of a normal vector nearly perpendicular to vector **b**, while β_2 angle delimits the region for the other normal vector away from the orthogonal position relative to **b**. The shaded zone in the figure corresponds to the singular case domain, where the bisectrix of the angle β_2 is defined based on an auxiliary angle γ, corresponding to the angle between $\mathbf{n}_0$ and **b**.

Fig. 6 presents an example of the Nagata patch interpolation applied to two piecewise linear elements, showing the influence of the selected values for the ε_1 and ε_2 parameters. The arrows represent the normal vectors and the dashed lines correspond to the piecewise linear interpolation of the geometry. The Nagata curves are presented by the thick continuous line and their uniform parametric coordinates ($\xi \in [0, 1]$ with an increment of 0.1) are represented using dashes over the curves.

The selected values for ε_1 and ε_2 have a strong impact both in the stability and the accuracy of the interpolation. The original formulation, without restrictions ($\varepsilon_1 = 0$ and $\varepsilon_2 = \infty$), is presented in Fig. 6(a). As highlighted in the detail in this figure, the Nagata curve obtained is non-uniform in the Cartesian coordinate system (see the dashes distribution over the Nagata curve). This non-uniformity can lead to convergence problems in the local contact search algorithms. On the other hand, when the selected value for ε_1 is too high and the one selected for ε_2 is too small, the quadratic Nagata interpolation leads to a linear interpolation for both piecewise elements, due to the very restrictive conditions imposed (see Fig. 6(c)). The correct choice of ε_1 and ε_2 values depends on the mesh topology (structured or unstructured) but it is mainly dictated by the type of vertex normal vector evaluation strategy adopted (exact or approximated vectors). They can be adjusted by the user in order to avoid interpolations with high localized curvature. However, according to the several tests performed in this study, using different piecewise linear meshes topologies and vertex normal vector evaluations, the values for ε_1 and ε_2 parameters can be selected based only on the normal vector evaluation strategy adopted. The parameter values selected can be always less restrictive when the exact normal vector is available. Nevertheless, the values selected for the other strategy can always be applied when the exact normal vector is available, leading to some avoidable linear interpolations. Furthermore, in order to avoid instability problems of the Nagata interpolation algorithm while keeping the accuracy, the maximum value for the β_1 angle is 4° (see Eq. (15)). In the example presented in Fig. 6(b) the admissible β_1 angle corresponds to 3°.

3. Interpolation applied to a curve: 2D geometry

This section is dedicated to the analysis of a 2D geometry, the circular arc. Although this is a simple geometry, this type of curve is always present in the 3D surfaces that define the most common tools for sheet metal forming process. Constant radius fillet surfaces and surfaces of revolution are typically adopted for constructing smooth tool surfaces [37,41].

The accuracy of the Nagata patch interpolation is evaluated using the radial and normal vector errors. The Cartesian coordinates of the Nagata interpolation for an arc of the circle with radius R are given by the position vector $\mathbf{x}(\xi)$, applying Eqs. (1) and (3). The Nagata curve approximates the arc of the circle with a radial error defined in each curve point by:

$$\delta_r(\xi) = \frac{(\mathbf{x}(\xi) - \mathbf{o}) \cdot \mathbf{n}_{\text{analytical}} - R}{R} \times 100[\%], \quad (16)$$

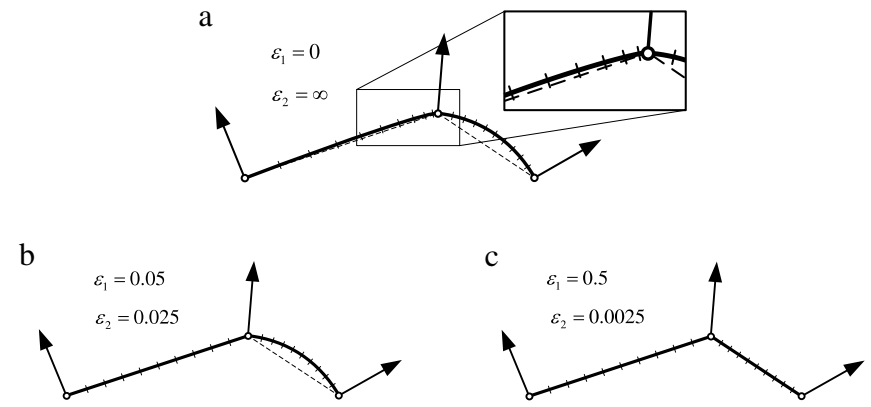

Fig. 6. Influence of ε_1 and ε_2 values in the Nagata patch interpolation behavior: (a) without restrictions presenting in detail the non-uniformity of the interpolation; (b) using admissible values; (c) using very restrictive values.

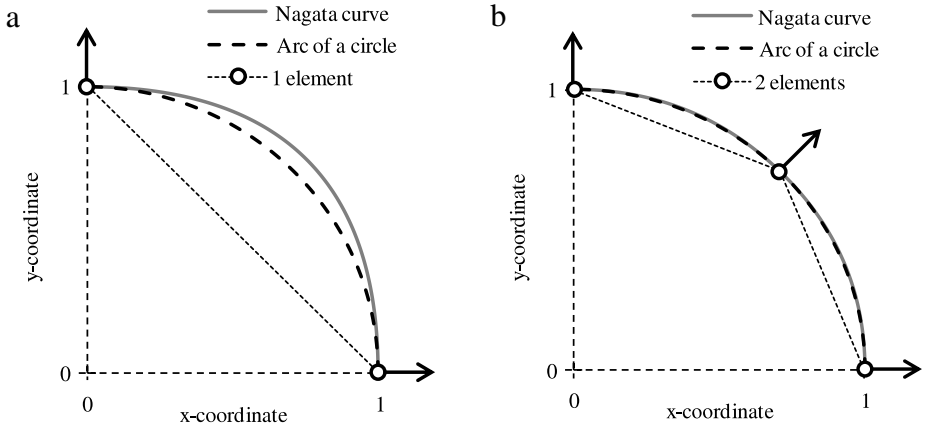

Fig. 7. Nagata patch and piecewise linear interpolation of a quarter-circle: (a) discretized by 1 element; (b) discretized by 2 elements.

where ξ satisfies the condition $0 \leq \xi \leq 1$, $\mathbf{o}$ is the position vector of the circle center and $\mathbf{n}_{\text{analytical}}$ is the unit normal vector to the arc of the circle evaluated using the analytic function. This error corresponds to the dimensionless distance between the Nagata curve and the arc of the circle defined by the analytical function, in the radial direction.

The Nagata curve approximates the arc of the circle with a normal vector error defined by:

$$\delta_{\text{n}}(\xi) = \cos^{-1}(\mathbf{n}_{\text{Nagata}}(\xi) \cdot \mathbf{n}_{\text{analytical}})[^\circ], \tag{17}$$

where ξ satisfies the condition $0 \leq \xi \leq 1$ and $\mathbf{n}_{\text{Nagata}}(\xi)$ is the unit normal vector to the Nagata curve interpolation, perpendicular to the direction calculated using Eq. (2). This error corresponds to the angular difference between the analytical and the approximated normal vector ($\mathbf{n}_{\text{Nagata}}$), expressed in degrees for each point of the curve.

A unit quarter-circle is used to analyze the error associated with the use of piecewise linear approximation and Nagata interpolation for its description. Besides the vertices coordinates, in order to apply the Nagata patch interpolation algorithm it is necessary to know the normal vector in each vertex. The required normal vector at each vertex was determined using the analytical function. Fig. 7(a) and (b) compares the analytical function with the Nagata patch and the piecewise linear interpolations, for the quarter-circle discretized with 1 and 2 linear elements, respectively. The Nagata patch interpolation results in a curve which is always outside the circle arc, with a maximum radial error at the mid point of the curve ($\xi = 0.5$) [19,42].

In order to study the influence of the mesh size on the interpolation error, the quarter-circle is equally divided in 1 to 10 circle arcs/elements, which correspond to a normalized arc length from 1.571 down to 0.157, respectively. The normalized arc length corresponds to the division of the arc length by the radius of the arc of the circle. Fig. 8 presents the comparison between the piecewise linear mesh and the Nagata patch interpolation, both in terms of maximum absolute radial error (Fig. 8(a)) and normal vector error (Fig. 8(b)). It is possible to observe in Fig. 8(a) that, in both approximations, the radial error decreases with the decrease of the normalized arc length, thus converging to the original geometry [36]. This figure also presents the trend lines between the modulus of maximum radial error and the normalized arc length, which shows that the order of convergence of the radial error is quadratic and quartic for the piecewise linear mesh and Nagata interpolation, respectively. Fig. 8(b) shows the evolution of the maximum error in the normal vector for both the piecewise linear mesh and the Nagata interpolation, as a function of the normalized arc length. The maximum error in the normal vector decreases with the decrease of the normalized arc length, similarly to the radial error. By analyzing the figure, it is possible to observe that the order of convergence of the normal vector error against the normalized arc length is linear and cubic for the piecewise linear mesh and Nagata interpolation, respectively. The correlation coefficients of the trend lines presented in Fig. 8, corresponding to the Nagata patch interpolations are not equal to one since the lengths of the Nagata curves and the arcs of circle are not equal (see Fig. 7). This analysis was performed taking into account the Nagata patch algorithm using the controlling methodologies presented in Section 2.3. However, due to the simple and regular geometry, the control conditions (see Eqs. (13) and (14)) are never activated. Thus, the same solution can be achieved using the original formulation [39].

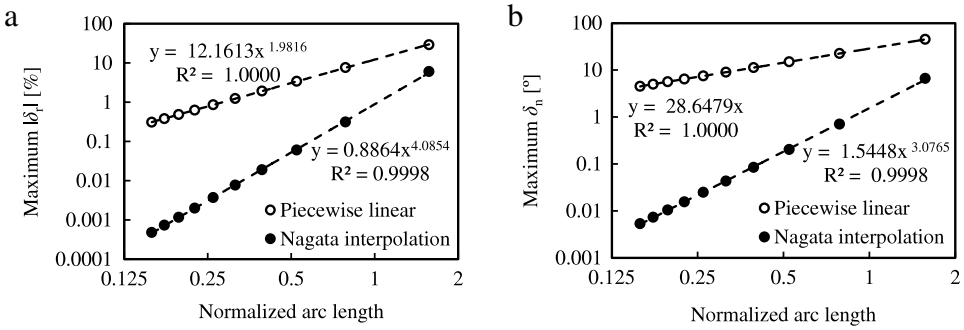

Fig. 8. Comparison between piecewise linear approximation and Nagata patch interpolation used to describe a quarter-circle: (a) maximum radial error modulus; (b) maximum normal vector error.

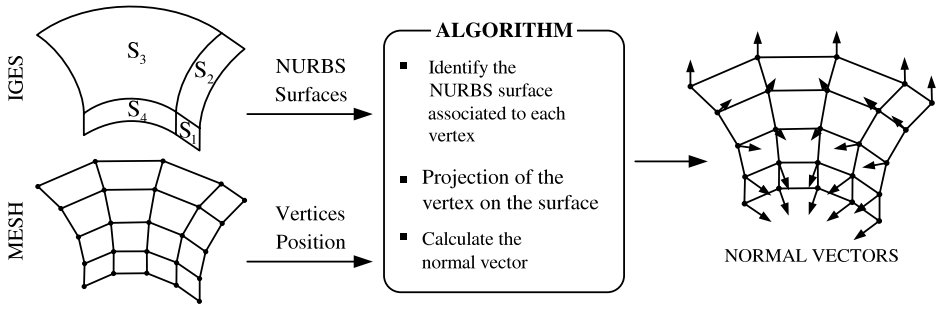

Fig. 9. Algorithm used to evaluate the vertex normal vector from CAD geometry based on trimmed NURBS surfaces.

4. Vertex normal vector evaluation

Typically, tool models are provided to Computer Aided Engineering (CAE) using exchange CAD formats. Thus, the information available in CAD model can be used to determine the normal vector in each vertex of the piecewise mesh, in order to apply the Nagata patch interpolation method. The proposed methodology to evaluate the normal vectors uses as inputs the neutral format IGES (Initial Graphics Exchange Specification) to extract the information concerning surface definition in the format of trimmed NURBS (Non Uniform Rational B-Spline) surfaces [43,44]. However, sometimes only the piecewise linear mesh of the tools surface is available, hence only the vertices' position and the connectivity of each element are known. Thus, it is important to develop a strategy that allows evaluating the vertex normal vector, based on the information available only in the piecewise linear mesh. Two approaches to estimate the normal vectors in the vertices of a piecewise mesh have been presented in the literature. The first approach is based on the determination of an interpolated surface on the vertex, such that the vertex normal vector is calculated as being equal to the surface normal vector [45–47]. The second approach consists on determining the weighted average of the normal vectors of facets adjacent to the vertex [48–51]. Due to its simplicity, the last approach was adopted in this work, where some algorithms for approximation of the vertex normal vector are presented.

4.1. Normal vector evaluated from CAD geometry

This algorithm is based on the tools definition using trimmed NURBS surfaces, which is a type of parametric surfaces commonly used in CAD software packages. The model definition using trimmed NURBS surfaces can be extracted from the standard IGES file format [44].

Fig. 9 presents schematically the proposed algorithm to evaluate the normal vector based on trimmed NURBS, which can be divided in three steps [39]. In order to determine the vertex normal vector, it is necessary to know the parametric coordinates (u, v) of each vertex of the piecewise linear mesh, on the model composed by trimmed NURBS surfaces. Since the tools can be described with a large number of trimmed NURBS surfaces, as shown in Fig. 9, first a global search is performed to select the surfaces associated to each vertex. The method used to perform the global search is based in the global contact search algorithm proposed by Oliveira et al. [17], which uses the coordinates of the middle point and each vertex of the NURBS surfaces. After the candidate surfaces pre-selection, the parametric coordinates (u, v) of each vertex are evaluated by vertex projection on the surfaces. The mathematical formulation of the projection algorithm adopted is presented in the Appendix, which allows determining the admissible projection point for the candidate surfaces. The selected surface is the one that has the closest projection point to the vertex. The normal vector, for each vertex of the piecewise linear mesh, is evaluated by the cross product of the two partial derivatives determined for the closest projection point.

4.2. Normal vector evaluated from piecewise linear mesh

When the CAD model geometry is not available, the normal vector in each mesh vertex is approximated by a weighted sum of the normal vectors of the facets defined by the reciprocal edges of the vertex. If n edges of the piecewise linear mesh are defined with vertex j, the estimative of the normal vector for this vertex involves the determination of the normal vector, $\mathbf{n}$, for each of the n facets. Fig. 10 presents the notation used to define the reciprocal edges as well as the normal vectors of each facet, when evaluating the normal vector of vertex j. All the methods presented in this section share the notion of weighting adjacent facet normal vectors, but they differ substantially in the weighting factor adopted [52].

4.2.1. Mean weighted equally

The algorithm presented in this subsection to estimate the vertex normal vector was introduced by Gouraud, in 1971. This

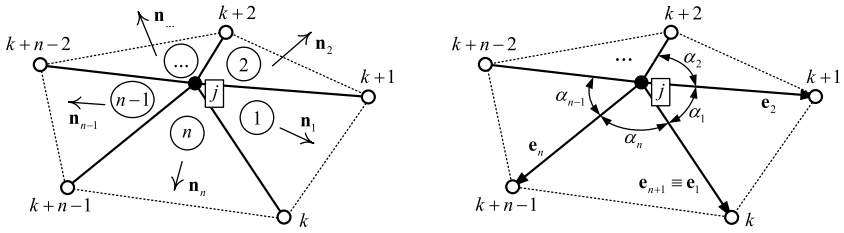

Fig. 10. Notation used to approximate the normal vector at vertex j shared by n piecewise facets.

algorithm will be referred as the mean weighted equally (MWE) algorithm, since the normal vector is determined as [48]:

$$\mathbf{n}_{\text{MWE}} \parallel \sum_{i=1}^{n} \mathbf{n}_i, \tag{18}$$

where $\mathbf{n}_i$ is the normal vector of the plane (facet) i and the summation is over all the n planes (facets) defined by vertex j (cf. Fig. 10). The symbol $\parallel$ indicates that the calculated vector is parallel to the unit vertex normal vector, since the required normal vector is always unitary.

4.2.2. Mean weighted by angle

While Gouraud (1971) [48] suggested equal weights, in 1998 Thürmer and Wüthrich proposed as weights the planes (facets) angles at the vertices. Defining as α_i the angle between the two edge vectors $\mathbf{e}_i$ and $\mathbf{e}_{i+1}$ of plane (facet) i sharing the vertex (see Fig. 10), the normal vector of the vertex is in this case determined as [49]:

$$\mathbf{n}_{\text{MWA}} \parallel \sum_{i=1}^{n} \alpha_i \mathbf{n}_i. \tag{19}$$

This will be referred as the mean weighted by angle (MWA) algorithm.

4.2.3. Mean weighted by sine and edge length reciprocals

The next four algorithms were introduced by Max, in 1999. The first algorithm, referred as the mean weighted by sine and edge length reciprocals (MWSELR), takes into account the differences in size of the adjacent edges to the vertex, assigning larger weights to smaller edges and higher angles between the two edge vectors. The normal vector to the vertex is determined as [50]:

$$\mathbf{n}_{\text{MWSELR}} \parallel \sum_{i=1}^{n} \frac{\mathbf{n}_i \sin(\alpha_i)}{|\mathbf{e}_i|\,|\mathbf{e}_{i+1}|}, \tag{20}$$

where $\mathbf{n}_i$, $\mathbf{e}_i$, $\mathbf{e}_{i+1}$ and α_i are defined as in the previous subsection.

4.2.4. Mean weighted by areas of adjacent triangles

The second algorithm, proposed by Max (1999) [50], incorporates the area of the triangle formed by the two edges incident on the vertex (whether the facet is triangular or not). Thus, this algorithm assigns larger weights to facets with larger area. The vertex normal vector is estimated using the following expression:

$$\mathbf{n}_{\text{MWAAT}} \parallel \sum_{i=1}^{n} \mathbf{n}_i\,|\mathbf{e}_i|\,|\mathbf{e}_{i+1}|\sin(\alpha_i) = \sum_{i=1}^{n} \mathbf{n}_i\,|\mathbf{e}_i \otimes \mathbf{e}_{i+1}|\,, \tag{21}$$

where $\mathbf{n}_i$, $\mathbf{e}_i$, $\mathbf{e}_{i+1}$ and α_i were defined in Section 4.2.2 and $\otimes$ represents the cross product of two vectors. This algorithm will be referred as the mean weighted by areas of adjacent triangles (MWAAT).

4.2.5. Mean weighted by edge length reciprocals

Max (1999) [50] also proposes to remove the sine factor in Eq. (20), which leads to an estimate of the vertex normal vector given as:

$$\mathbf{n}_{\text{MWELR}} \parallel \sum_{i=1}^{n} \frac{\mathbf{n}_i}{|\mathbf{e}_i|\,|\mathbf{e}_{i+1}|}, \tag{22}$$

where $\mathbf{n}_i$, $\mathbf{e}_i$ and $\mathbf{e}_{i+1}$ are defined as in Eq. (19). This algorithm will be referred as the mean weighted by edge length reciprocals (MWELR) and assigns larger weights to smaller edges.

4.2.6. Mean weighted square root of edge length reciprocals

The last algorithm proposed by Max (1999) [50] is similar to the MWELR, with the addition of a square root:

$$\mathbf{n}_{\text{MWRELR}} \parallel \sum_{i=1}^{n} \frac{\mathbf{n}_i}{\sqrt{|\mathbf{e}_i|\,|\mathbf{e}_{i+1}|}}, \tag{23}$$

where $\mathbf{n}_i$, $\mathbf{e}_i$ and $\mathbf{e}_{i+1}$ are defined as in Eq. (19). This will be referred as the mean weighted by square root of edge length reciprocals (MWRELR) algorithm.

4.2.7. Methodology to correct the vertex normal vector approximation

The above mentioned algorithms are suitable and offer good results for regular piecewise linear meshes of smooth surfaces with high level of continuity [52]. However, typically sheet metal forming tools present a combination of flat and curved surface regions. In the boundary between these two types of surfaces none of the presented algorithms show the same level of accuracy, particularly in coarse meshes. Therefore, in order to reduce the normal vector approximation error in those regions, we propose a methodology that corrects the normal vector in the vertices that share a flat surface.

The central idea of the proposed methodology is based on the comparison between the normal vector of each piecewise linear element and the corresponding approximated normal vectors at their vertices. Hence, when a vertex belonging to an element presents an approximated normal vector equal to the normal vector of the own element, the implemented algorithm imposes that all vertices of this element should present the normal vector of the own element. Fig. 11 presents an example of a 2D geometry composed by two transition zones between flat and curved surfaces, which is representative of 3D surface cross sections, usually present in tool geometries involved in the numerical simulation of sheet metal forming processes. For this 2D geometry, discretized with the piecewise mesh shown in Fig. 11, the application of the MWE algorithm to approximate the normal vector in each vertex (denoted by $\mathbf{n}_{(i)}$) leads to normal vector errors of 11.25° in the vertices 2 and 4. In fact, regardless of the normal vector approximation algorithm adopted, the evaluated normal vectors in these vertices are influenced by the normal vector of the piecewise elements 2 and 3, leading to high error values in the normal vector approximation. The application of the proposed methodology significantly improvements the normal vector of vertices 2 and 4, as shown in Fig. 11 through the normal vectors denoted by $\mathbf{n}'_{(i)}$. In fact, in this example the application of the correction methodology leads to a null error in the approximation

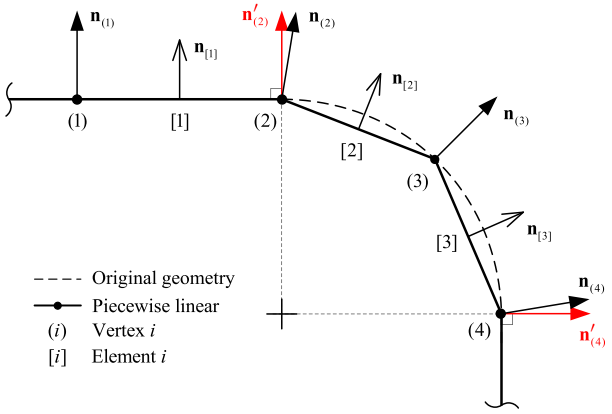

Fig. 11. Effect of the proposed correction methodology in the normal vector approximation of vertices 2 and 4. Corrected normal vectors are denoted by $\mathbf{n}'_{(i)}$.

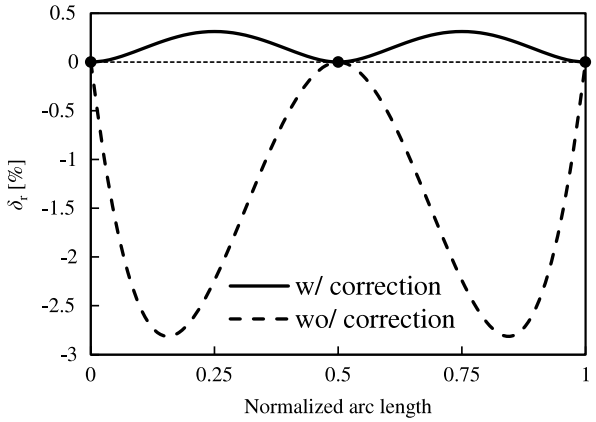

Fig. 12. Radial error resulting from the Nagata interpolation of a circular arc using the vertex normal vectors evaluated through the MWE algorithm. Effect of the proposed correction methodology in the interpolation accuracy.

of the normal vector for all vertices. In order to highlight the influence of the normal vectors accuracy in the Nagata patch interpolation, Fig. 12 presents the radial error resulting from the interpolation of the circular arc using the normal vectors estimated by the MWE algorithm, employing or not the proposed correction methodology. The range of the radial error obtained with the interpolation that uses the normal vectors without correction is almost ten times higher than the one obtained with the correction methodology.

5. Nagata patches applied to tool description

The Nagata patch interpolation error analysis performed considering the unit quarter circular arc in Section 3 can be used as a guideline for the description of 3D surfaces, such as the cylinder, sphere and the torus. Previous results obtained considering these simple surfaces [39], indicate that the radial error in the cylinder is dictated only by the discretization in the circumferential direction, where the maximum error value attained is equal to the one obtained for the corresponding circular arc. In case of the sphere, discretized by triangular piecewise linear elements, the maximum radial error is dictated by the maximum edge length, which is easily related with the normalized arc length presented in Fig. 8(a). Finally, the torus presents two principal curvatures that increase its complexity. When quadrilateral piecewise linear elements are used to describe the torus surface, the maximum positive radial error is located at hyperbolic points, while the maximum negative error arises in elliptic points. The limit value of radial error is

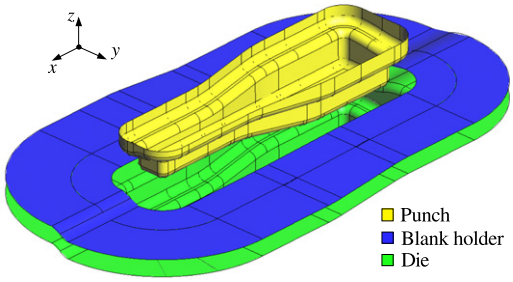

Fig. 13. Tools geometry, defined by trimmed NURBS surfaces, employed in the sheet metal forming process [53].

mainly dictated by the number of piecewise linear elements in the major radius direction [39].

In this section, the Nagata patch interpolation is applied to describe a sheet metal forming tool. Fig. 13 presents the tools geometry (punch, blank holder and die) selected for this analysis, which correspond to the forming of a complex shape part [53]. The analysis is performed considering only the die, since the punch and the blank holder present a geometry which can be obtained by off-set of the die surfaces. The die has a high complex shape, combining plane, cylinder, sphere and torus surfaces. Its length, width and height are 596, 320 and 75 mm, respectively, and the minor curvature radius present in the geometry is 8 mm.

The information required for the Nagata patch interpolation algorithm is only the position vector and the normal vector of each vertex of the mesh. The position vectors are determined from the piecewise linear mesh of the geometry under study, which can be composed by triangular or quadrilateral elements. It is important to mention that the surface orientation dictates the elements connectivity and, consequently the normal vector orientation. At this stage, the information available in CAD model is used to determine the normal vector in each vertex of the piecewise mesh.

The piecewise linear meshes used in this study to discretize the die model are divided in two topological groups: structured and semi-structured meshes. In each of these groups both triangular and quadrilateral elements are used. The coarse meshes are obtained considering a maximum of 3 elements along each circular arc, while the fine meshes use a maximum of 4 elements. Fig. 14 presents the coarser structured piecewise mesh obtained with triangular elements (Mesh T1), as well as a detail of the four different meshes in a zone with more complex shape. Meshes T1 and T2 are structured while the T3 and T4 are semi-structured. Fig. 15 presents the coarser structured piecewise linear mesh composed by quadrilateral elements (Mesh Q1), as well as a detail of the same zone for the other meshes that considers quadrilateral elements. Meshes Q1 and Q2 are structured while Q3 is semi-structured. In this case, the two structured meshes are composed by triangular elements in the die corners, as shown in Fig. 15, due to the simplicity of describing a 3-sided surface with triangular elements generated symmetrically [37]. The main features of both triangular and quadrilateral piecewise linear meshes are shown in Table 1. For the models composed only by triangular elements, the number of elements and vertices is similar for both structured and semi-structured meshes, in order to be able to perform a direct comparison. However, it is not possible to adopt the same strategy for the quadrilateral meshes, due to the high increase in the number of elements in semi-structured meshes. Globally, the quadrilateral models present fewer elements that the triangular models, which can be more suitable for contact search algorithms. Nevertheless, in general, the quadrilateral mesh generation is more complex and time consuming.

In order to also evaluate the accuracy of the piecewise linear meshes, the Nagata patch interpolation is applied to each piecewise mesh using a null value for the coefficients that add the curvature to the patch, i.e. using linear interpolation.

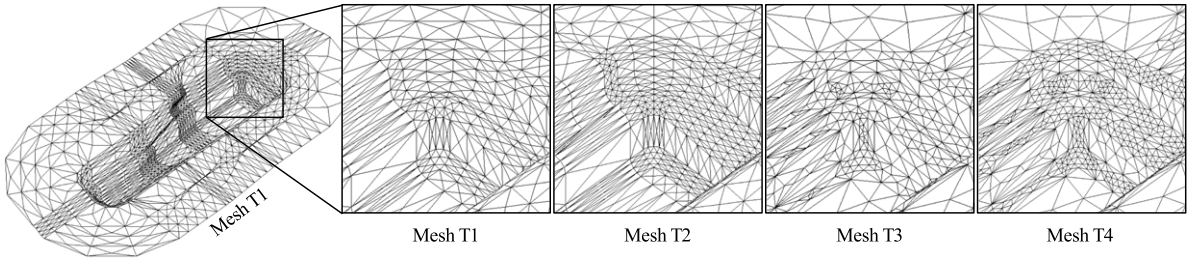

Fig. 14. Die model described by triangular piecewise elements and detail of the same zone for the 4 models: T1 and T2 structured and T3 and T4 semi-structured meshes.

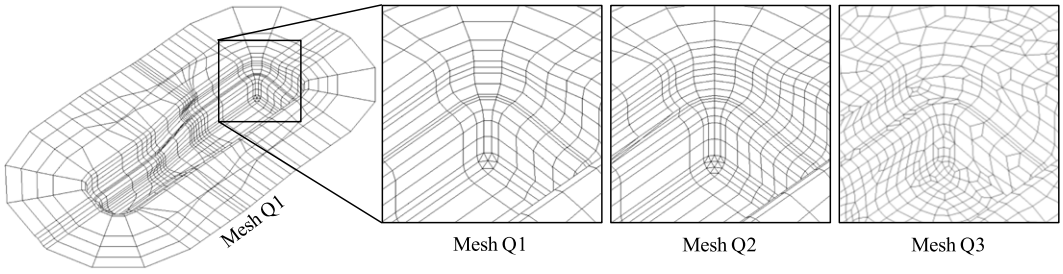

Fig. 15. Die model described by quadrilateral piecewise elements and detail of the same zone for the 3 models: Q1 and Q2 structured and Q3 semi-structured meshes.

Table 1
Main characteristics of the piecewise meshes used to describe the die tool.

Mesh characteristic	Piecewise triangular mesh				Piecewise quadrilateral mesh		
	Structured		Semi-structured		Structured		Semi-structured
	T1	T2	T3	T4	Q1	Q2	Q3
Number of elements	4196	6464	4058	6562	1262	1892	3807
Number of vertices	2130	3271	2052	3310	1276	1899	3854

5.1. Error in the Nagata patch interpolation

In order to evaluate the accuracy of the Nagata patch interpolation applied to the die, two types of errors are analyzed. The first one is the shape error that is evaluated as follows:

$$\delta_{\text{Shape}}(\eta,\zeta) = (\mathbf{P}-\mathbf{P}')\cdot\mathbf{n}_{\text{CAD}} = (\mathbf{x}_{\text{Nagata}}(\eta,\zeta)-\mathbf{P}')\cdot\mathbf{n}_{\text{CAD}} = -\mathbf{d}\cdot\mathbf{n}_{\text{CAD}}, \quad (24)$$

where $\mathbf{P}\equiv\mathbf{x}_{\text{Nagata}}(\eta,\zeta)$ is the position vector of each point where the error is evaluated, $\mathbf{P}'$ is the orthogonal projection of point $\mathbf{P}$ on the NURBS surface (see Appendix) and n_{CAD} is the unit normal vector of the NURBS surface at the point $\mathbf{P}'$. This error corresponds to the signed distance $\mathbf{d}$ between a point on the Nagata patch and the NURBS surface, measured in the orthogonal direction and expressed in the same length units that the geometry is defined (in this case millimetres). In order to highlight the graphical interpretation of Eq. (24), Fig. 16 shows the error calculated in two points $\mathbf{P}_1$ and $\mathbf{P}_2$, where the first point presents a negative shape error while the second has a positive one. The C^0 continuity of the discretized surface is guarantee both in the piecewise mesh and the Nagata patch interpolation. Therefore, the shape error is a continuous function and is possible to plot it as a continuous distribution.

The second type of error studied is the normal vector error, given by:

$$\delta_{\text{n}}(\eta,\zeta) = \cos^{-1}(\mathbf{n}_{\text{Nagata}}(\eta,\zeta)\cdot\mathbf{n}_{\text{CAD}})[^\circ], \quad (25)$$

where $\mathbf{n}_{\text{Nagata}}(\eta,\zeta)$ is the unit normal vector of each point $\mathbf{P}$ of the Nagata patch where the error is evaluated. This error corresponds to the angle between the normal vector evaluated through the CAD model geometry, obtained at the point $\mathbf{P}'$of the NURBS surface,

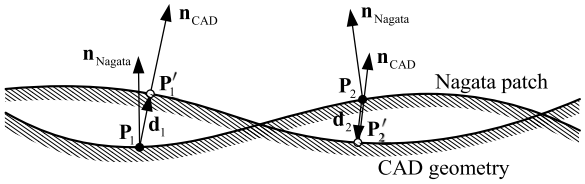

Fig. 16. Evaluation of the shape and normal vector errors for two points on the Nagata patch interpolation: point $\mathbf{P}_1$ with a negative shape error ($\mathbf{d}_1\cdot\mathbf{n}_{\text{CAD}}>0$) and $\mathbf{P}_2$ with a positive shape error ($\mathbf{d}_2\cdot\mathbf{n}_{\text{CAD}}<0$).

and the normal vector of the Nagata patch, expressed in degrees. Fig. 16 also presents the variables necessary to evaluate this error, for both $\mathbf{P}_1$ and $\mathbf{P}_2$. However, unlike the shape error, the normal vector error is not a continuous function. According to the Nagata patch algorithm, the normal vector is continuous inside each patch, and in the vertices, if a singular case is not attained. Nevertheless, in the edges the C^1 continuity condition is not verified. To overcome this limitation Nagata proposed a G^1 Nagata patch interpolation [38]. However, this algorithm leads to much more complex interpolations and the C^0 continuity guaranteed by the original Nagata patch interpolation is sufficient, even for high-precision engineering [54]. In the next section, both errors are analyzed for the selected tool geometry, described by either triangular or quadrilateral piecewise linear meshes and Nagata patches.

5.2. Accuracy of the Nagata patch interpolation using normal vectors evaluated from CAD geometry

This section presents the comparison between the piecewise linear mesh and the corresponding Nagata patch interpolation,

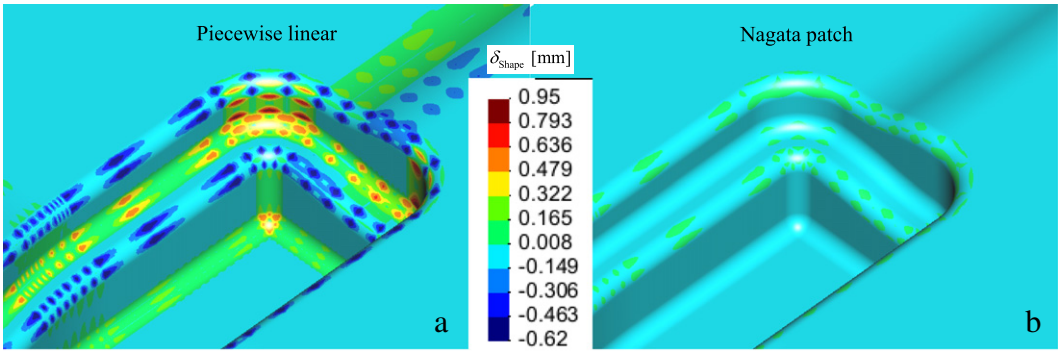

Fig. 17. Shape error distribution in the tool model approximated by: (a) triangular piecewise linear mesh T1 and; (b) Nagata patch interpolation.

Table 2
Comparison of shape and normal vector error between triangular piecewise linear approximation and Nagata patch interpolation.

Triangular mesh	Piecewise linear mesh				Nagata patch			
	Shape error [mm]			Normal vector error [°]	Shape error [mm]			Normal vector error [°]
	Min.	Max.	Range	Max.	Min.	Max.	Range	Max.
T1	−0.617	0.954	1.57	43.9	−0.090	0.096	0.19	18.1
T2	−0.278	0.538	0.82	25.2	−0.048	0.048	0.10	11.2
T3	−1.250	1.199	2.45	43.9	−0.290	0.182	0.47	19.5
T4	−0.707	0.940	1.65	39.3	−0.095	0.095	0.19	13.8

both in terms of shape and normal vector errors, when the normal vectors in each vertex are provided from the CAD geometry. This analysis is performed for all models, 4 triangular and 3 quadrilateral piecewise linear meshes, applying the Nagata patch algorithm using the control coefficient values of $\varepsilon_1 = 0.036$ and $\varepsilon_2 = 0.020$. These values were chosen as the minimum ones to control both type of piecewise linear meshes, i.e. triangular and quadrilateral, when using the normal vectors evaluated from CAD geometry.

5.2.1. Triangular patches

The error analysis, both in the piecewise mesh and the Nagata patch interpolation, is performed using the maximum, minimum and range of the shape error and the maximum normal vector error. Table 2 presents these limit values for both the piecewise linear mesh and the triangular Nagata patch interpolation. Using the Nagata patch interpolation to smooth the piecewise meshes, the error range decrease significantly, for both types of error analyzed. The range of the shape error in the Nagata patches is always at least 80% lower than the one in the piecewise linear meshes, whatever the mesh description considered. The same behavior is observed in the normal vector error, where the range in the Nagata patches is always at least 55% lower than the one in the piecewise meshes.

The distribution of the shape error allows observing the zones where the maximum error values are attained. This distribution is obtained by constructing a fine grid of points over each patch and calculating the shape error in each point. Due to the nearly geometrical symmetry of the model, the distribution of the shape error is performed only in an area of the die geometry, where the limit values of the shape error are attained. Fig. 17 shows the comparison of shape error distribution between the piecewise linear mesh T1 and the corresponding Nagata patch interpolation. The application of the Nagata patch interpolation in the triangular mesh leads to a strong decrease of the shape error in all geometry, but particularly in the cylindrical zones, following the same trend predicted for the circular arc (see Fig. 8 (a)). In the case of the triangular mesh T1, the interpolation results in a shape error range 88 % lower than the piecewise linear mesh.

The distribution of both errors is also analyzed in a selected cross section of the die geometry, where the shape is more

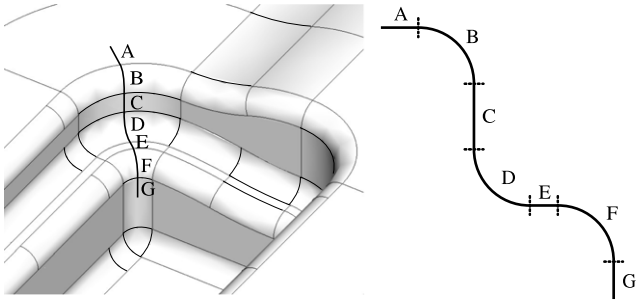

Fig. 18. Location of the tool cross section where the error distributions are analyzed and detail of its original geometry.

complex. The cross section, shown in Fig. 18, is divided in seven segments labeled from A to G. This analysis is performed only for the coarser structured mesh T1, which is representative of the results obtained with the other piecewise meshes. Fig. 19 shows, for both piecewise linear mesh and Nagata patch interpolation, the evolution of the shape error along the selected cross section. The difference of error values between both approaches is evident, with the maximum value attained in the Nagata patch approach being 10 times less than in the piecewise mesh. Both in the piecewise mesh and in the Nagata patch interpolation, the maximum value of shape error for this geometry is attained in this section. For the piecewise linear mesh the maximum value is attained in region C while for the Nagata patch interpolation the maximum values occur in region B, corresponding to a more complex hyperbolic region. Section C corresponds to a parabolic region, for which the error is mainly dictated by the circumferential element size, i.e. the normalized arc length [39].

The normal vector error distribution for both approaches, in the same cross section, is shown in Fig. 20. As previously mentioned, in order to guarantee the stability of the Nagata patch interpolation, the restrictions to the original Nagata formulation presented in the Section 2.3, were implemented. Thus, some patches do not satisfy the imposed boundary conditions, leading to linear interpolations. This is visible in region B of the cross section (Figs. 19 and 20), where the error distributions are overlapping for the region corresponding to the connection element with region A, which

Table 3
Comparison of shape and normal vector error between quadrilateral piecewise linear approximation and Nagata patch interpolation.

Quadrilateral mesh	Piecewise linear mesh				Nagata patch			
	Shape error [mm]			Normal vector error [°]	Shape error [mm]			Normal vector error [°]
	Min.	Max.	Range	Max.	Min.	Max.	Range	Max.
Q1	−0.888	1.458	2.35	28.0	−0.063	0.172	0.23	8.7
Q2	−0.406	0.783	1.19	18.5	−0.020	0.048	0.07	4.9
Q3	−1.220	1.303	2.52	42.0	−0.149	0.147	0.30	10.0

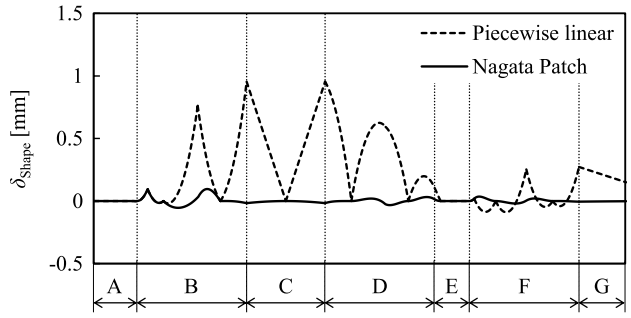

Fig. 19. Shape error distributions along the cross section in the triangular mesh T1.

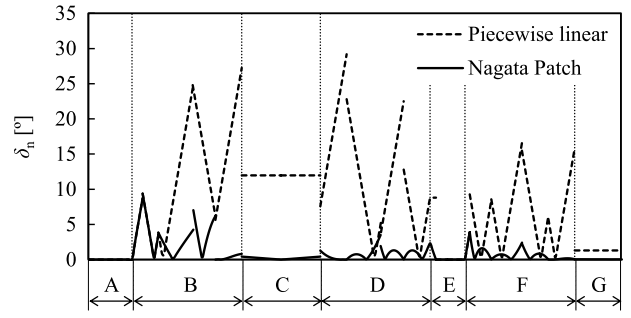

Fig. 20. Normal vector error distributions along the cross section in the triangular mesh T1.

indicates the adoption of the linear interpolation for this element. The maximum normal vector error is not attained in this cross section. For the piecewise linear mesh, the maximum value is attained in a region located in the die shoulder, which presents two elements with a much larger size along the circumferential direction than along the edge direction, which connect to the addendum surface. On the other hand, the maximum error attained in the Nagata patch interpolation is located in the boundary vertices between region A and B, due to the linear interpolation imposed for the patches that share these vertices. Thus, in specific cases the adoption of the proposed controlling methodologies can result in an increase of both errors, when compared with the original Nagata patch interpolation algorithm. Nevertheless, considering the cross section under analysis, the maximum error value attained for the piecewise mesh is 29.2°, while in the Nagata interpolation is only 9.4°, thus 68% lower.

5.2.2. Quadrilateral patches

The limit values of both studied errors for the three quadrilateral element meshes are presented in Table 3. The shape error range in the Nagata interpolation is always at least 88% lower than in the piecewise linear mesh, even for the semi-structured mesh Q3. The error in the normal vector is also reduced when the interpolation is applied, being always at least 69% lower than the one attained in the piecewise linear mesh.

Fig. 21 shows the comparison between the piecewise linear mesh and the Nagata patch interpolation in terms of shape error distribution, for the quadrilateral mesh Q1. The error range is smaller in the Nagata patch interpolation compared with the convectional piecewise linear mesh, particularly in coarser discretized zones. For this structured mesh, the Nagata interpolation presents a shape error range 90% lower than the piecewise mesh, similar to the result obtain with the triangular mesh T1.

The evolution of both the shape and normal vector errors in the piecewise linear mesh and in the Nagata interpolation, along the selected cross section presented in Fig. 18, is shown in Figs. 22 and 23, respectively. The maximum value of both errors is attained in this cross section, but in different locations. In the piecewise mesh the maximum value of both errors are located in region D (elliptic points), while the region B (hyperbolic points) is where are located the maximum errors in the Nagata patch interpolation.

The maximum shape error value in the piecewise linear mesh is 1.46 mm, while in the Nagata patch interpolation is 0.17 mm, thus about 88% lower. It should be mentioned that the shape error value in the piecewise mesh would forbidden its application in the numerical simulation of this sheet metal forming process, since it is close to the value of the gap between the die and the punch. While the piecewise linear mesh attains a maximum of 27.9° for the normal vector error, the Nagata patch interpolation presents a maximum value of 8.7°, thus 69% lower than the piecewise mesh. This difference is similar to the one obtained for the triangular mesh T1 in this section. However, unlike for the triangular mesh T1, the interpolation result obtained in this section

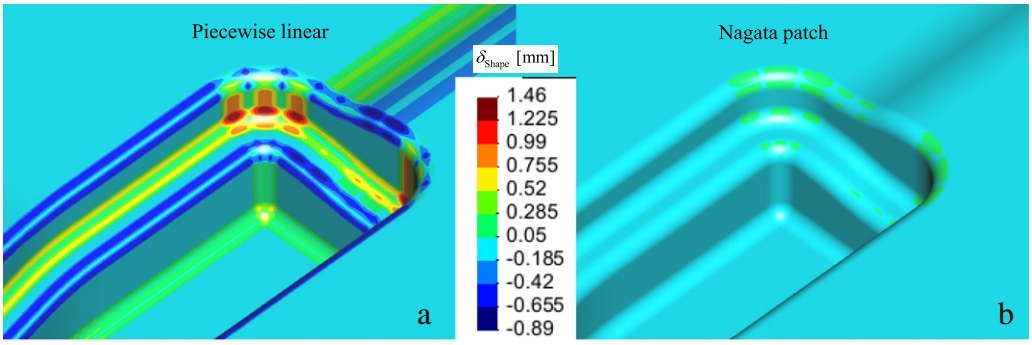

Fig. 21. Shape error distribution in the tool model approximated by: (a) triangular piecewise linear mesh Q1 and; (b) Nagata patch interpolation.

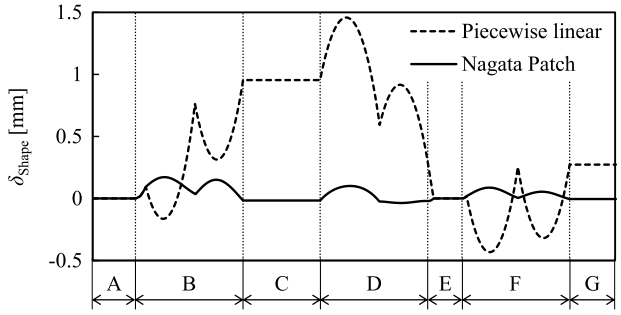

Fig. 22. Shape error distributions along the cross section in the quadrilateral mesh Q1.

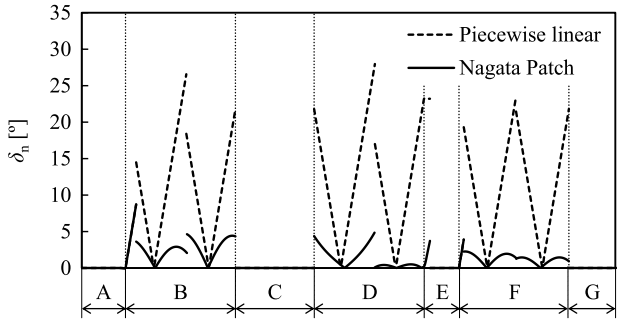

Fig. 23. Normal vector error distributions along the cross section in the quadrilateral mesh Q1.

with the quadrilateral mesh Q1 is not affected by the restrictions introduced in the original Nagata patch interpolation, keeping the boundary conditions for all vertices of the elements along this section. This is a result of the reduced number of piecewise linear elements (see Table 1) and also of the type of element. In fact, finer refinements typically lead to more problems concerning inversion of surface orientation. These problems also arise more frequently in triangular elements, since they are more flexible in the surface geometry representation. The inversion of surface orientation problem is minimized in piecewise meshes with the element edges aligned along the geometry main curvatures, as is the case of the majority of the zones of the quadrilateral models studied in this work.

5.3. Error in the normal vectors approximation

In order to evaluate the efficiency of the normal vector estimative algorithms presented in Section 4.2, they were all applied to the previously presented die piecewise linear meshes. The error in normal vector approximation is evaluated in each vertex of the mesh, using the following definition:

$$\theta = \cos^{-1}(\mathbf{n}_{CAD} \cdot \mathbf{n}_{algorithmic})[^\circ], \tag{26}$$

where $\mathbf{n}_{algorithmic}$ is the unit normal vector evaluated in each vertex of the mesh using the different algorithms previously presented and $\mathbf{n}_{CAD}$ is the unit normal vector of the CAD model (NURBS surface). Thus, this error is calculated only in the vertices of the piecewise mesh and corresponds to the angular difference between the CAD and the approximated normal vectors, expressed in degrees.

The cumulative distributions of the normal vector error were studied. In this section these results are presented only for meshes T1 and Q1, since they are representative of the global behavior. Fig. 24 presents the cumulative distribution of the normal vector error approximation for mesh T1. The analysis of this figure allows observing the improvement in the normal vectors

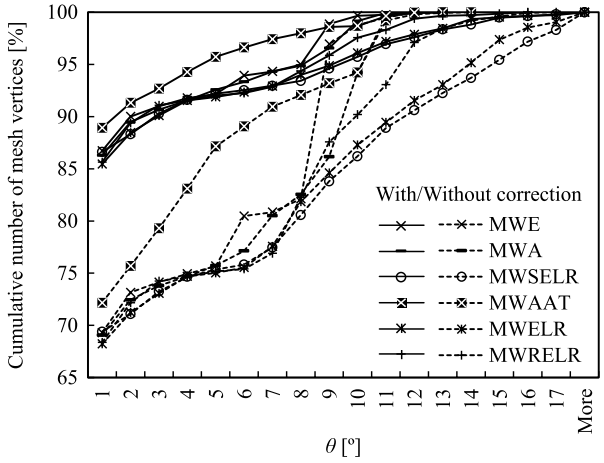

Fig. 24. Distribution of normal vector approximation error obtained for mesh T1, with and without applying the correction methodology to the different normal vector approximation algorithms.

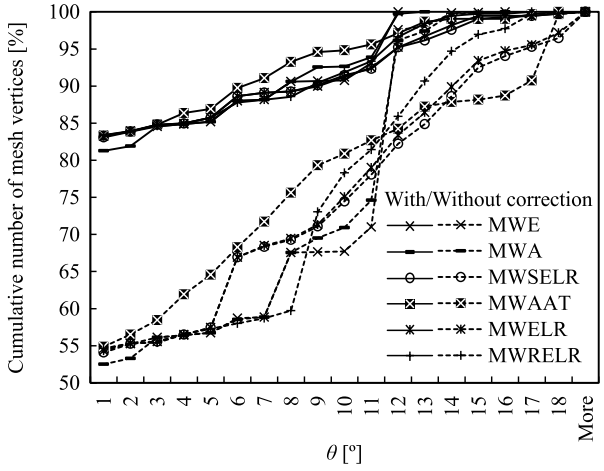

Fig. 25. Distribution of normal vector approximation error obtained for mesh Q1, with and without applying the correction methodology to the different normal vector approximation algorithms.

approximation when the correction methodology proposed in the Section 4.2.7 is applied. In fact, the correction leads to a higher number of vertices with a small error in the normal vector approximation, regardless of the algorithm used. The same cumulative distribution is presented in Fig. 25 for the normal vector error approximation obtained in mesh Q1. Also, in this case it is visible that the correction methodology clearly improves the error distribution. Therefore, the methodology proposed to improve the normal vector approximation is suitable for both triangular and quadrilateral structured meshes. For both triangular and quadrilateral structured meshes, the MWAAT algorithm provides the best solution in terms of the error distribution, before and after applying the correction methodology (sees Figs. 24 and 25). This behavior is due to the fact that the selected geometry comprises big flat areas. In fact, during the tools description process, these areas can be discretized with a low number of piecewise elements, leading to a coarse mesh. Since the MWAAT algorithm adopts the area of element as weight, bigger elements present higher weight than others. Thus, the nodes in the boundary between flat and curve surfaces will present an approximated normal vector closer to the normal vector of the flat surface, i.e. the exact normal vector.

Fig. 26 presents the maximum error attained in the normal vector approximation for each die model considered, with and

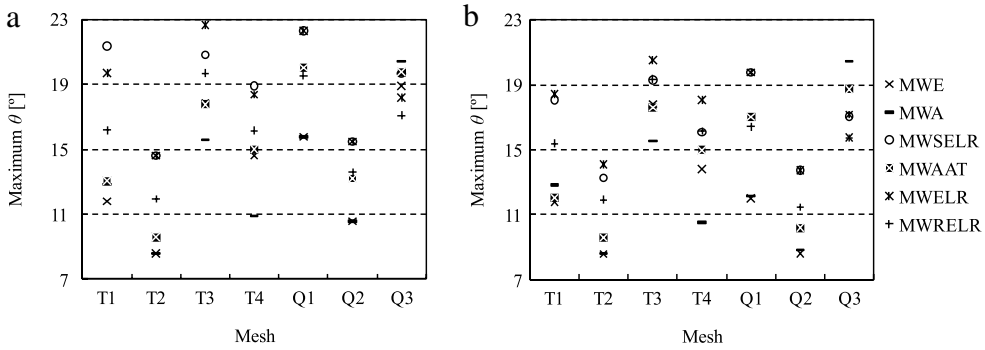

Fig. 26. Maximum normal vector approximation error attained for each mesh using the different algorithms: (a) without applying the correction methodology; (b) applying the correction methodology.

without the correction methodology applied. The effect of the correction method in the maximum normal vector approximation error is lower than in the error distribution due to the local characteristic of the first one. Whatever the approximation algorithm used or the type of mesh, the maximum error attained after correction is always inferior or equal to the one obtained without correction (see Fig. 26). The maximum error is always reached in vertices located in the boundary between different surfaces, since the C^1 continuity is not attained at those boundaries. However, a better distribution of the normal vector approximation does not directly imply a lower value for the maximum error. In both triangular and quadrilateral meshes, the increase in the number of elements (piecewise mesh refinement) implies a decrease of the maximum error, while for the same number of elements the best approximation is attained by structured meshes. Fig. 26(b) shows that for structured meshes, when the correction method is applied, the MWE algorithm always gives the best solution in terms of maximum error attained due to the use of equal weights for all elements. Except for the quadrilateral mesh Q3, the MWA algorithm presents always a good solution even for triangular semi-structured meshes, where it is clearly the best solution, while the MWELR algorithm provides the worst approximation. The MWA algorithm leads to good results for both triangular and quadrilateral meshes that present small angles (always less than 90°) between the element edges. This is always more easy to assure in triangular models as well in quadrilateral structured models.

5.4. Accuracy of the Nagata patch interpolation using approximated normal vectors

This section analyses the effect of the normal vector approximation in the Nagata patch interpolation accuracy. The analysis is performed comparing the Nagata patch interpolation using approximated normal vectors with the one obtained using the normal vectors evaluated from the CAD geometry as well as with the piecewise linear mesh. The approximated normal vectors considered in this analysis always take into account the correction methodology proposed, since it always renders inferior error in the normal vector estimative. Due to normal vector approximation, the range of singular cases is increased in order to control the Nagata patch interpolation. For structured meshes the values used for the coefficients are $\varepsilon_1 = 0.070$ and $\varepsilon_2 = 0.015$, while for the semi-structured meshes the value of ε_1 is increased to 0.075. These values were chosen as the minimum ones necessary to control the Nagata patch interpolation of the piecewise linear meshes, when using approximated normal vectors.

Figs. 27 and 28 presents the shape error range and the maximum normal vector error in the Nagata patch interpolation, respectively. The figures include the results for all studied meshes and present the values attained for the piecewise linear meshes

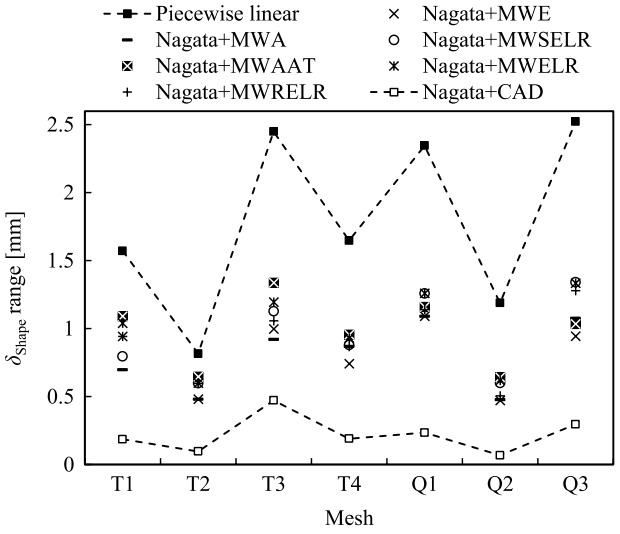

Fig. 27. Shape error range obtained in the Nagata patch interpolation for each mesh using the different normal vector approximation algorithms. Comparison with range values attained for piecewise linear mesh and Nagata interpolations based on the exact vertex normal vector.

(labeled Piecewise linear), for the Nagata patch interpolation using the normal vectors evaluated from the CAD geometry (labeled Nagata+CAD) and for the Nagata patch with approximated normal vectors, using the different algorithms. The use of normal vectors evaluated from the CAD geometry in the Nagata patch interpolation gives always the best approximation, in terms of both errors under analyses. On the contrary, the definition of the die geometry with the piecewise linear meshes leads to the worst approximation in terms of both errors. There is only one exception to this global behavior, which occurs when the MWAAT algorithm is applied to mesh T4.

In order to analyze the influence of the normal vectors approximation in the Nagata patch interpolation, the shape and normal vector error distributions along the selected cross section, presented in Fig. 18, are determined for mesh Q1. This mesh is selected because it allows a better comparative analysis of the normal vector estimative algorithms since it is the coarser mesh. Both quadrilateral structured meshes, Q1 and Q2, are composed by elements with angles between edges near 90° with a small dispersion, thus some algorithms to approximate the normal vector present a similar behavior, as shown in Figs. 25 and 26. The MWA algorithm presents results similar to the MWE algorithm (see Eqs. (18) and (19)), while the MWSELR gives a similar error to the one attained with the MWELR algorithm (see Eqs. (20) and (22)). Therefore, the analysis is performed considering only the following three algorithms: MWE, MWAAT and MWELR.

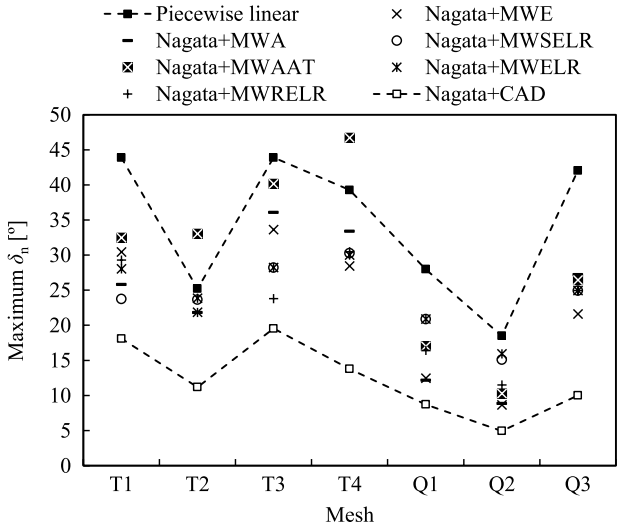

Fig. 28. Maximum normal vector error obtained in the Nagata patch interpolation for each mesh using the different normal vector approximation algorithms. Comparison with the values attained for piecewise linear mesh and Nagata interpolations based on the exact vertex normal vector.

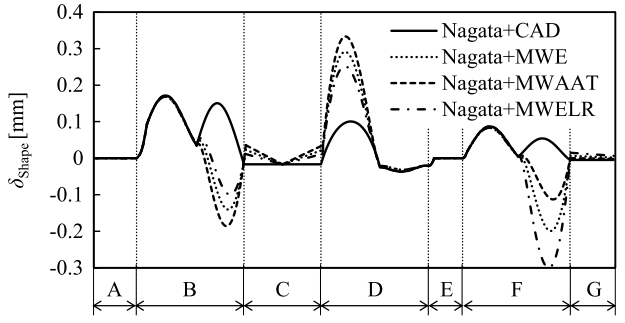

Fig. 29. Shape error distributions along the cross section in the quadrilateral mesh Q1 for different normal vector approximation algorithms.

The shape and normal vector error distributions of the Nagata patch interpolation along the selected cross section, for mesh Q1, are presented in Figs. 29 and 30, respectively. The use of approximated normal vectors in the Nagata patch interpolation leads to an increase of the maximum value of both errors. This increase is only observed in some elements due to a less accurate approximation of the normal vector in at least one vertex of the element. The vertices that present higher value of normal vector error are characterized by being in the boundary between two surfaces with non null curvature. This is observable in Figs. 29 and 30, where only the elements that share a boundary between the regions B–C, C–D and F–G present a significant error relatively to the Nagata patch that uses normal vectors evaluated from CAD geometry. The same figures show that the use of the MWE algorithm in the Nagata patch interpolation gives always a solution between the ones obtained using the MWAAT and the MWELR algorithms. The MWAAT algorithm uses a weight proportional to the edge size of the elements, while the weight used in the MWELR algorithm is inversely proportional to the edge size. Thus, application of these two algorithms gives opposite solutions both in the shape and normal vector error of the Nagata patch interpolation.

In order to obtain an overview of the error distributions in the Nagata patches obtained using approximated normal vectors, a grid of points is constructed over all patches, and the errors are calculated in each point. This study is performed for mesh T1, for which the limit error values attained are already known (see

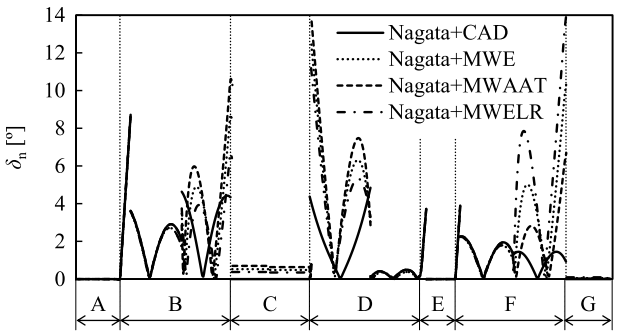

Fig. 30. Normal vector error distributions along the cross section in the quadrilateral mesh Q1 for different normal vector approximation algorithms.

Figs. 27 and 28). Figs. 31 and 32 show the shape and normal vector error distribution in the Nagata patch interpolation, respectively. The analysis is performed considering the piecewise linear mesh as well as the Nagata patch interpolations using vertex normal vectors evaluated both from CAD model and applying the MWE algorithm. In both figures, the coordinates of the points where the error is evaluated are projected in the *x*-axis, which is the direction of greater length, in order to plot the distribution in a 2D scatter. Fig. 31 shows that most points of the piecewise linear mesh present a shape error range less than 1.2 mm, while most points of the Nagata patch interpolation using vertex normal vectors from CAD geometry present a range inferior to 0.05 mm. The use of the MWE algorithm to approximate the normal vectors gives a shape error range less than 0.5 mm, for most points. The Nagata patch interpolation using the MWE algorithm present a maximum normal vector error inferior to 15°, for most points. Comparing Figs. 31 and 32 it is possible to observe that for the Nagata patch interpolation using the normal vectors from CAD geometry, the regions where the shape error range attains the highest value corresponds to the ones where the maximum normal vector error also occurs. This is a consequence of the geometric complexity of this region (transition between flat surface and torus) and the coarse description adopted. The comparison of Figs. 27 and 28 with 31 and 32 allows confirming the local characteristic of the maximum range of the shape error and the normal vector error. Thus, the Nagata patch interpolation, even using approximated normal vectors, leads to an improved geometric description when compared to the piecewise linear mesh.

6. Conclusions

In this work the Nagata patch interpolation is applied to a complex sheet metal forming tool description using both normal vectors evaluated from CAD geometry or approximated using different algorithms, all based on the weighted average of the normal vectors of facets adjacent to the vertex. The singular case domain of the original Nagata patch interpolation algorithm is extended in order to avoid inversion of curve orientation or high localized curvature, situations that must be avoided when using this type of approach for contact surface description. The complex tool is discretized with triangular and quadrilateral elements, using both structured and semi-structured meshes. The shape and normal vector errors are evaluated and compared for the piecewise linear mesh, the Nagata patch interpolation using normal vectors evaluated from CAD geometry and the Nagata patch interpolated using approximated normal vectors. Based on the results analysis it is possible to observe:

- The introduction of the proposed correction methodology to the original Nagata patch interpolation leads to a more robust algorithm without degradation of the shape accuracy.

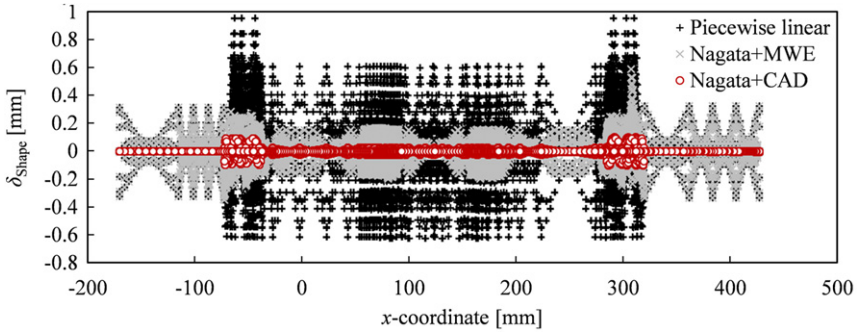

Fig. 31. Shape error distribution for the mesh T1 model, represented considering the coordinates of the geometry evaluated points projected in the *x*-axis.

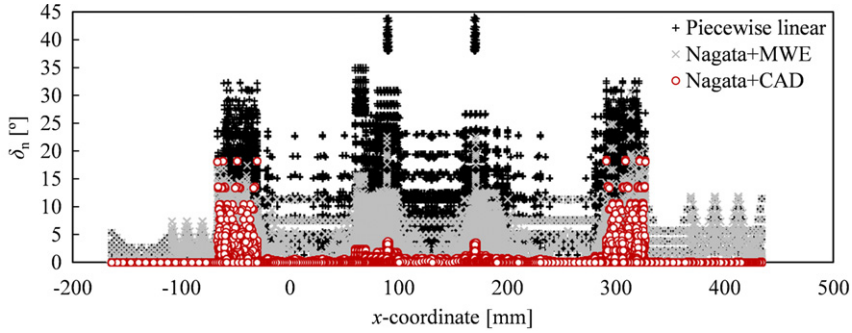

Fig. 32. Normal vector error distribution for the mesh T1 model, represented considering the coordinates of the geometry evaluated points projected in the *x*-axis.

The adopting of this correction methodology can leads to an increase of both shape and normal vector errors in specific elements where it is applied. Nevertheless, the Nagata patch interpolation always presents a shape error at least 80% lower than the piecewise linear mesh and a normal vector error at least 55% lower.

- The use of approximated normal vectors in Nagata patch interpolation can be improved by adopting a methodology that corrects the normal vector in vertices that share a flat surface. Using this methodology, the different algorithms for vertex normal vector approximation can even lead to similar cumulative normal vector approximation error distributions, particularly for structured meshes.
- The maximum vertex normal vector approximation error is influenced by the mesh typology (i.e. triangular or quadrilateral), the mesh topology (i.e. structured or semi-structure) and the complexity of the original geometry. Thus, it is not possible to select an algorithm for vertex normal vector approximation which renders accurate results in all situations. Nevertheless, when compared with the other algorithms considering the different piecewise linear meshes, the MWE algorithm presents a lower average of the maximum normal vector approximation error.
- The Nagata patch interpolation using normal vectors evaluated from CAD geometry always renders the more accurate interpolation, both in terms of shape and normal vector errors. The use of approximated normal vectors in the Nagata patch algorithm reduces the accuracy, in particular for coarse piecewise meshes.

In brief, the use of Nagata patch to describe tool surfaces in the numerical simulation of sheet metal forming processes is a good alternative in terms of accuracy relatively to the widely used piecewise linear meshes. Furthermore, its characteristic reduced interpolation degree allows keeping the simplicity in the mathematical formulation of the contact search treatment.

Acknowledgments

The authors gratefully acknowledge the financial support of the Portuguese Foundation for Science and Technology (FCT) under Project PTDC/EME-TME/103350/2008 by FEDER through the program QREN (COMPETE: FCOMP-01-0124-FEDER-010301). The first author is also grateful to the FCT for the Ph.D. grant SFRH/BD/69140/2010. The authors also would like to thank the editors and anonymous reviewers for their constructive suggestions.

Appendix. Projection of a point on a NURBS surface

Considering a generic point $\mathbf{P}(x, y, z)$ that will be orthogonally projected on a NURBS surface $\mathbf{S}(u, v)$, in order to obtain the projection point $\mathbf{P}'$. According to Stadler et al., the distance vector $\mathbf{r}(u, v)$, which connects the point $\mathbf{P}$ to an arbitrary point $\mathbf{S}(u, v)$ of the surface, is defined as [25]:

$$\mathbf{r}(u, v) = \mathbf{S}(u, v) - \mathbf{P}(x, y, z) \tag{A.1}$$

and its evaluation requires the following orthogonal conditions:

$$\begin{cases} f(u, v) = \mathbf{S}_u(u, v) \cdot \mathbf{r}(u, v) = 0 \\ g(u, v) = \mathbf{S}_v(u, v) \cdot \mathbf{r}(u, v) = 0, \end{cases} \tag{A.2}$$

where $\mathbf{S}_u(u, v) = \partial\mathbf{S}(u, v)/\partial u$ and $\mathbf{S}_v(u, v) = \partial\mathbf{S}(u, v)/\partial v$ indicate the first partial derivatives of the surface. In order to solve the above nonlinear system of equations, the Newton–Raphson method can be applied, leading to the incremental solution vector:

$$[\delta_i] = \begin{bmatrix} \Delta u_i \\ \Delta v_i \end{bmatrix}, \tag{A.3}$$

where the Jacobian matrix of system of equations presented in (A.2) is:

$$[J_i] = \begin{bmatrix} f_u & f_v \\ g_u & g_u \end{bmatrix}_i = \begin{bmatrix} |\mathbf{S}_u|^2 + \mathbf{r} \cdot \mathbf{S}_{uu} & \mathbf{S}_u \cdot \mathbf{S}_v + \mathbf{r} \cdot \mathbf{S}_{uv} \\ \mathbf{S}_u \cdot \mathbf{S}_v + \mathbf{r} \cdot \mathbf{S}_{uv} & |\mathbf{S}_v|^2 + \mathbf{r} \cdot \mathbf{S}_{vv} \end{bmatrix}_i \tag{A.4}$$

and the residual vector is:

$$[\kappa_i] = -\begin{bmatrix} f(u_i, v_i) \\ g(u_i, v_i) \end{bmatrix}, \tag{A.5}$$

where the second order surface partial derivatives of the surface are given by $\mathbf{S}_{uu} = \partial^2\mathbf{S}(u, v)/\partial u^2$, $\mathbf{S}_{vv} = \partial^2\mathbf{S}(u, v)/\partial v^2$ and $\mathbf{S}_{uv} = \partial^2\mathbf{S}(u, v)/\partial u\partial v$. The initial values u_0 and v_0 should be given *a priori*, influencing the convergence speed. In the adopted approach the initial values are estimated based on the minimum distance between $\mathbf{P}$ and a set of points of the surface, equally spaced in the parametric domain. This enables to write the iterative solution procedure for step i as:

$$[J_i][\delta_i] = [\kappa_i] \tag{A.6}$$

and to update according to:

$$\begin{bmatrix} u_{i+1} \\ v_{i+1} \end{bmatrix} = \begin{bmatrix} u_i \\ v_i \end{bmatrix} + [\delta_i]\,. \tag{A.7}$$

The necessary derivatives of the NURBS surface $\mathbf{S}(u, v)$ can be obtained with:

$$\frac{\partial^{k+l}}{\partial^k u \partial^l v}\mathbf{S}(u, v) = \sum_{i=0}^{n}\sum_{j=0}^{m} N_{i,p}^{(k)}(u) N_{j,p}^{(l)}(v)\mathbf{P}_{i,j} \tag{A.8}$$

with

$$N_{i,p}^{(k)}(u) = p\left(\frac{N_{i,p-1}^{(k-1)}}{u_{i+p} - u_i} - \frac{N_{i+1,p-1}^{(k-1)}}{u_{i+p+1} - u_{i+1}}\right). \tag{A.9}$$

References

[1] Gantar G, Ljevar M, Kuzman K. The use of numerical simulations in the development of tools for the sheet-metal parts of cars. J Mech Eng 2001;47:605–14.

[2] Makinouchi A. Sheet metal forming simulation in industry. J Mater Process Technol 1996;60:19–26.

[3] Haepp HJ, Rohleder M. FE simulation of sheet metal forming-state of the art in automotive industry. Adv Mater Res 2005;6–8:13–8.

[4] Erman Tekkaya A. State-of-the-art of simulation of sheet metal forming. J Mater Process Technol 2000;103:14–22.

[5] Zhou D, Wagoner RH. Development and application of sheet-forming simulation. J Mater Process Technol 1995;50:1–16.

[6] Chenot J-L, Fourment L, Mocellin K. Numerical treatment of contact and friction in FE simulation of forming processes. J Mater Process Technol 2002;125–126:45–52.

[7] Christensen PW, Klarbring A, Pang JS, Stromberg N. Formulation and comparison of algorithms for frictional contact problems. Int J Numer Methods Eng 1998;42:145–73.

[8] Svensson M, Mattiasson K. Three-dimensional simulation of hemming with the explicit FE-method. J Mater Process Technol 2002;128:142–54.

[9] Menezes LF, Neto DM, Oliveira MC, Alves JL. Improving computational performance through HPC techniques: case study using DD3IMP in-house code. AIP Conf Proc 2011;1353:1220–5.

[10] Gantar G, Pepelnjak T, Kuzman K. Optimization of sheet metal forming processes by the use of numerical simulations. J Mater Process Technol 2002;130–131:54–9.

[11] Hallquist JO, Wainscott B, Schweizerhof K. Improved simulation of thin-sheet metalforming using LS-DYNA3D on parallel computers. J Mater Process Technol 1995;50:144–57.

[12] Hughes TJR, Cottrell JA, Bazilevs Y. Isogeometric analysis: CAD, finite elements, NURBS, exact geometry and mesh refinement. Comput Methods Appl Mech Eng 2005;194:4135–95.

[13] De Lorenzis L, Temizer İ, Wriggers P, Zavarise G. A large deformation frictional contact formulation using NURBS-based isogeometric analysis. Int J Numer Methods Eng 2001;87:1278–300.

[14] Zhuang S, Lee MG, Keum YT, Kim JH, Wagoner RH. Improved contact procedure for implicit finite element sheet forming simulation. Int J Numer Methods Eng 2010;83:1759–79.

[15] Yang B, Laursen TA, Meng X. Two dimensional mortar contact methods for large deformation frictional sliding. Int J Numer Methods Eng 2005;62:1183–225.

[16] Benson DJ, Hallquist JO. A single surface contact algorithm for the post-buckling analysis of shell structures. Comput Methods Appl Mech Eng 1990;78:141–63.

[17] Oliveira MC, Alves JL, Menezes LF. Improvement of a frictional contact algorithm for strongly curved contact problems. Int J Numer Methods Eng 2003;58:2083–101.

[18] Yastrebov VA, Cailletaud G, Feyel F. A local contact detection technique for very large contact and self-contact problems: sequential and parallel implementations. In: Zavarise G, Wriggers P, editors. Trends in computational contact mechanics. LNACM, vol. 58. Berlin: Springer-Verlag; 2011. p. 227–51.

[19] Hama T, Nagata T, Teodosiu C, Makinouchi A, Takuda H. Finite-element simulation of springback in sheet metal forming using local interpolation for tool surfaces. Int J Mech Sci 2008;50:175–92.

[20] Hachani M, Fourment L. A 3D contact smoothing method based on quasi-C^1 interpolation and normal voting–application to 3D forging and rolling. AIP Conf Proc 2010;1252:487–95.

[21] Yang DY, Yoo DJ, Song IS, Lee JH. Investigation into tool surface description for finite element analysis of three-dimensional sheet metal forming process. J Mater Process Technol 1994;45:267–73.

[22] Santos A, Makinouchi A. Contact strategies to deal with different tool descriptions in static explicit FEM of 3-D sheet metal forming simulation. J Mater Process Technol 1995;50:277–91.

[23] Yoo DJ, Song IS, Yang DY, Lee JH. Rigid-plastic finite element analysis of sheet metal forming processes using continuous contact treatment and membrane elements incorporating bending effects. Int J Mech Sci 1994;36:513–46.

[24] Konyukhov A, Schweizerhof K. Incorporation of contact for high-order finite elements in covariant form. Comput Methods Appl Mech Eng 2009;198:1213–23.

[25] Stadler M, Holzapfel GA, Korelc J. C^n continuous modelling of smooth contact surfaces using NURBS and application to 2D problems. Int J Numer Methods Eng 2003;57:2177–203.

[26] Stadler M, Holzapfel GA. Subdivision schemes for smooth contact surfaces of arbitrary mesh topology in 3D. Int J Numer Methods Eng 2004;60:1161–95.

[27] Heege A, Alart P. A frictional contact element for strongly curved contact problems. Int J Numer Methods Eng 1996;39:165–84.

[28] Wriggers P, Krstulovic-Opara L, Korelc J. Smooth C^1-interpolations for two-dimensional frictional contact problems. Int J Numer Methods Eng 2001;51:1469–95.

[29] El-Abbasi N, Meguid SA, Czekanski A. On the modelling of smooth contact surfaces using cubic splines. Int J Numer Methods Eng 2001;50:953–67.

[30] Padmanabhan V, Laursen TA. A framework for development of surface smoothing procedures in large deformation frictional contact analysis. Finite Elem Anal Des 2001;37:173–98.

[31] Puso MA, Laursen TA. A 3D contact smoothing method using Gregory patches. Int J Numer Methods Eng 2002;54:1161–94.

[32] Wriggers P. Finite element algorithms for contact problems. Arch Comput Methods Eng 1995;2:1–49.

[33] Shim HB, Suh EK. Contact treatment algorithm for the trimmed NURBS surface. J Mater Process Technol 2000;104:200–6.

[34] Farouki RT. Closing the gap between CAD model and downstream application. SIAM News 1999;32(5):303–19.

[35] Menezes LF, Teodosiu C. Three-dimensional numerical simulation of the deep-drawing process using solid finite elements. J Mater Process Technol 2000;97:100–6.

[36] Nagata T. Simple local interpolation of surfaces using normal vectors. Comput Aided Geom Design 2005;22:327–47.

[37] Lin J, Ball AA, Zheng JJ. Surface modelling and mesh generation for simulating superplastic forming. J Mater Process Technol 1998;80-81:613–9.

[38] Nagata T. Smooth local interpolation of surfaces using normal vectors. J Appl Math 2010;2010:24. (Open access journal).

[39] Neto DM, Oliveira MC, Menezes LF. Nagata patch interpolation algorithms: strategies towards sheet metal forming tools description in CAE. Saarbrücken: VDM Verlag; 2010.

[40] Boschiroli M, Fünfzig C, Romani L, Albrecht G. A comparison of local parametric C^0 Bézier interpolants for triangular meshes. Comput Graph UK 2011;35:20–34.

[41] Lin J, Ball AA, Zheng JJ. Approximating circular arcs by Bézier curves and its application to modelling tooling for FE forming simulations. Int J Mach Tools Manuf 2001;41:703–17.

[42] Neto DM, Oliveira MC, Alves JL, Menezes LF. Local interpolation for tools surface description. AIP Conf Proc 2010;1252:479–86.

[43] Neto DM, Oliveira MC, Menezes LF, Alves JL. Evaluating the vertex normal vector in polyhedral mesh using the IGES file format, in: Andrade-Campos A, Lopes N, Valente RAF, Varum H, editors. YIC 2012, First ECCOMAS young investigators conference on computational methods in applied sciences. University of Aveiro, Aveiro, 2012, p. 33.

[44] Initial graphics exchange specification: IGES 5.3. IGES/PDES Organization. U.S. Product Data Association, 1996.

[45] Meek DS, Walton DJ. On surface normal and Gaussian curvature approximations given data sampled from a smooth surface. Comput Aided Geom Design 2000;17:521–43.
[46] Kim H, Kim H. Computing vertex normals from arbitrary meshes. In: Mastorakis NE, Demiralp M, Mladenov V, Bojkovic Z, editors. Proceedings of the 9th international conference on signal processing, computational geometry and artificial vision. Wisconsin: World Scientific and Engineering Academy and Society; 2009. p. 68–72.
[47] Can A, Ünüvar A. Five-axis tool path generation for 3D curves created by projection on B-spline surfaces. Int J Adv Manuf Technol 2010;49:1047–57.
[48] Gouraud H. Continuous shading of curved surfaces. IEEE Trans Comput 1971; 20:623–9.
[49] Thürmer G, Wüthrich C. Computing vertex normals from polygonal facets. J Graphics Tools 1998;3:43–6.
[50] Max N. Weights for computing vertex normals from facet normals. J Graphics Tools 1999;4:1–6.
[51] Page DL, Sun Y, Koschan AF, Paik J, Abidi MA. Normal vector voting: crease detection and curvature estimation on large, noisy meshes. Graph Models 2002;64:199–229.
[52] Jin S, Lewis RR, West D. A comparison of algorithms for vertex normal computation. Visual Comput 2005;21:71–82.
[53] Rohleder M, Roll K, Menezes LF, Oliveira MC, Andersson A, Krantz F. Standardization of input output data for benchmark tests, Digital Die Design Systems (3DS) IMS 1999 000051. Work Package 2. Task 3, 2002.
[54] Lin W, Watanabe Y, Morita S, Uehara Y, Ohmori H. Development of a V-CAM system and its application to manufacturing. J Japan Soc Abrasive Technol 2007;51:290–5.